INL/EXT-13-30056

Investigation of the Performance of D_2O-Cooled High-Conversion Reactors for Fuel Cycle Calculations

Hikaru Hiruta
Gilles Youinou

September 2013

The INL is a U.S. Department of Energy National Laboratory
operated by Battelle Energy Alliance

DISCLAIMER

This information was prepared as an account of work sponsored by an agency of the U.S. Government. Neither the U.S. Government nor any agency thereof, nor any of their employees, makes any warranty, expressed or implied, or assumes any legal liability or responsibility for the accuracy, completeness, or usefulness, of any information, apparatus, product, or process disclosed, or represents that its use would not infringe privately owned rights. References herein to any specific commercial product, process, or service by trade name, trade mark, manufacturer, or otherwise, does not necessarily constitute or imply its endorsement, recommendation, or favoring by the U.S. Government or any agency thereof. The views and opinions of authors expressed herein do not necessarily state or reflect those of the U.S. Government or any agency thereof.

INL/EXT-13-30056

Investigation of the Performance of D2O-Cooled High-Conversion Reactors for Fuel Cycle Calculations

Hikaru Hiruta
Gilles Youinou

September 2013

Idaho National Laboratory
Reactor Physics Analysis & Design Department
Idaho Falls, Idaho 83415

Prepared for the
U.S. Department of Energy
Office of Nuclear Energy
Under U.S. Department of Energy-Idaho Operations Office
Contract DE-AC07-05ID14517

SUMMARY

This report presents FY13 activities for the analysis of D_2O cooled tight-pitch High-Conversion PWRs (HCPWRs) with U-Pu and Th-U fueled cores aiming at break-even or near breeder conditions while retaining the negative void reactivity. The analyses are carried out from several aspects which could not be covered in FY12 activities. SCALE 6.1 code system is utilized, and a series of simple 3D fuel pin-cell models are developed in order to perform Monte Carlo based criticality and burnup calculations.

The performance of U-Pu fueled cores with axial and internal blankets is analyzed in terms of their impact on the relative fissile Pu mass balance, initial Pu enrichment, and void coefficient. In FY12, Pu conversion performances of D_2O-cooled HCPWRs fueled with MOX were evaluated with small sized axial/internal DU blankets (~4cm of axial length) in order to ensure the negative void reactivity, which evidently limits the conversion performance of HCPWRs. In this fiscal year report, the axial sizes of DU blankets are extended up to 30 cm in order to evaluate the amount of DU necessary to reach break-even and/or breeding conditions. Several attempts are made in order to attain the milestone of the HCPWR designs (i.e., break-even condition and negative void reactivity) by modeling of HCPWRs under different conditions such as boiling of D_2O coolant, MOX with different ^{235}U enrichment, and different target burnups.

A similar set of analyses are performed for Th-U fueled cores. Several promising characteristics of ^{233}U over other fissile like ^{239}Pu and ^{235}U, most notably its higher fission neutrons per absorption, η, in thermal and epithermal ranges combined with lower η in the fast range than ^{239}Pu allows Th-U cores to be taller than MOX ones. Such an advantage results in 4% higher relative fissile mass balance than that of U-Pu fueled cores while retaining the negative void reactivity until the target burnup of 51 GWd/t. Several other distinctions between U-Pu and Th-U fueled cores are identified by evaluating the sensitivity coefficients of k_{eff}, mass balance, and void coefficient.

The effect of advanced iron alloy cladding (i.e., FeCrAl) on the performance of Pu conversion in MOX fueled cores is studied instead of using standard stainless-steel cladding. Variations in clad thickness and coolant-to-fuel volume ratio are also exercised. The use of FeCrAl instead of SS as a cladding alloy reduces the required Pu enrichment and improves the Pu conversion rate primarily due to the absence of nickel in the cladding alloy that results in the reduction of the neutron absorption. Also the difference in void coefficients between SS and FeCrAl alloys is nearly 500 pcm over the entire burnup range.

The report also shows sensitivity and uncertainty analyses in order to characterize D_2O cooled HCPWRs from different aspects. The uncertainties of integral parameters (k_{eff} and void coefficient) for selected reactor cores are evaluated at different burnup points in order to find similarities and trends respect to D_2O-HCPWR.

CONTENTS

FIGURES

TABLES

ACRONYMS

PWR	Pressurized Water Reactor
HCWR	High-Conversion Water Reactor
HCPWR	High-Conversion Pressurized Water Reactor
BWR	Boiling Water Reactor
BOC	Beginning Of Cycle
EOC	End Of Cycle
CANDU	CANada Deuterium Uranium
SFR	Sodium cooled Fast Reactor
MOX	Mixed OXide fuel
UOX	Uranium OXide fuel
DU	Depleted Uranium
ΔPu_f	Relative fissile Pu mass balance
$\Delta^{233}U$	Relative ^{233}U mass balance
EFPD	Equivalent Full Power Days
W/F ratio	Water (coolant)-to-Fuel ratio
SS	Stainless Steel
σ	Standard deviation

FUEL CYCLE OPTIONS CAMPAIGN

INVESTIGATION OF THE PERFORMANCE OF D_2O-COOLED HIGH-CONVERSION REACTORS FOR FUEL CYCLE CALCULATIONS

1. Introduction

This document reports the FY13 activities for the analysis of D_2O-cooled high-conversion PWRs (HCPWRs). A number of designs and analyses of high-conversion water reactors (HCWR) have been performed by several research groups in order to establish a sustainable fuel-cycle, which could be the alternative to fast reactor fuel cycle options [1-7]. The design targets of such reactors are to obtain high Pu conversion ratio while retaining the negative void reactivity. The vast majority of these studies considered only light water (H_2O) whereas there has been limited number of studies done for heavy water (D_2O) as a means to harden the neutron spectrum. The reason could be its unique but similar characteristics to the light water, as well as its higher cost.

The heavy water has very small neutron capture cross-section, and deuterium is one the lightest elements, second only to hydrogen, hence allowing reaching criticality even with natural uranium. However, in order to take advantage of its good neutron moderation properties, it is necessary to have large volumes of D_2O because the elastic scattering cross-section of deuterium in the slowing-down energy range is only about 4 barns against about 20 barns for hydrogen. The difference in the neutron elastic scattering cross-sections of H_2O and D_2O is the reason for the different sizes of PWRs and CANDUs; for the same power CANDUs need to be larger than PWRs to allow enough space for the neutrons to slow down to the thermal energy. Such unique characteristics in the heavy water could be suitable for the design of HCWR.

One of aspects necessary to achieve the design target of high-conversion reactors is the hardening of neutron spectrum in order to increase the conversion of ^{238}U into ^{239}Pu. One can obtain the harder spectrum by either reducing the water-to-fuel volume ratio (i.e., tightening the fuel pin pitch) or using the coolants that are more transparent to neutron than H_2O. For instance, if H_2O is replaced by D_2O in a PWR or BWR lattice, the resulting neutron spectrum will be substantially harder (see Figure 1). The sodium, of course, is more transparent to neutron than H_2O and D_2O. However, the resulting neutron spectrum will be very close to that of voided core, which indicates that void reactivity of sodium cooled core is always small and likely to be positive in MOX fueled core. Thus, in order to retain negativity in its void reactivity, the neutron leakage from the core must be increased by means of geometric configuration (increasing surface-to-volume ratio of the core). The neutron spectra in HCWRs are not as hard as those in sodium-cooled reactors (see Figure 2). These reactors can be characterized as fast systems; however, there will be large spectrum shift due to voiding of cores, which could be the potential sign to retain negative void reactivity.

This report presents the continuation of the activity started from FY12 [8] and further investigates the D_2O-cooled HCPWRs neutronics design from several aspects. In FY12, Pu conversion performances of D_2O-cooled HCPWRs fueled with MOX were evaluated with small sized axial/internal DU blankets (~4cm of axial length) in order to ensure the negative void reactivity, which evidently limits the conversion performance of HCPWRs. In this fiscal year report, the axial sizes of DU blankets are extended up to 30 cm in order to evaluate the amount of DU necessary to reach break-even and/or breeding conditions. Several attempts are made in order to attain the milestone of the HCPWR designs

(i.e., break-even condition and negative void reactivity) by modeling of HCPWRs under different conditions such as boiling of D_2O coolant, different target burnups, MOX with different ^{235}U enrichment, and different type and thickness of fuel claddings. In FY13, Th-U fueled core is also investigated which could be the promising approach for the sustainable fuel cycle. Section 2 of this report explains the computational method used for the analysis of HCPWRs. Sections 3 and 4 evaluate the performance of D_2O-cooled HCPWRs fueled with U-Pu and Th-U cycles, respectively. Section 4 also addresses the difference between these two types of fuel via simple sensitivity analyses. Section 5 studies the effect of advanced ferritic alloy cladding on the performance of Pu conversion in MOX fueled cores instead of using standard stainless-steel cladding. Variations in clad thickness and coolant-to-fuel volume ratio are also exercised. Section 6 demonstrates the fuel-cycle process based on D_2O-cooled HCPWRs that simulates through the recycling of Pu and fabrication of MOX fuel until it reaches equilibrium condition. Section 7 performs sensitivity and uncertainty analyses of k_{eff} and voids coefficients of HPWR and addresses some similarities to other familiar systems such as sodium cooled reactor (SFR) and PWR. Finally, the conclusion is provided in Section 8.

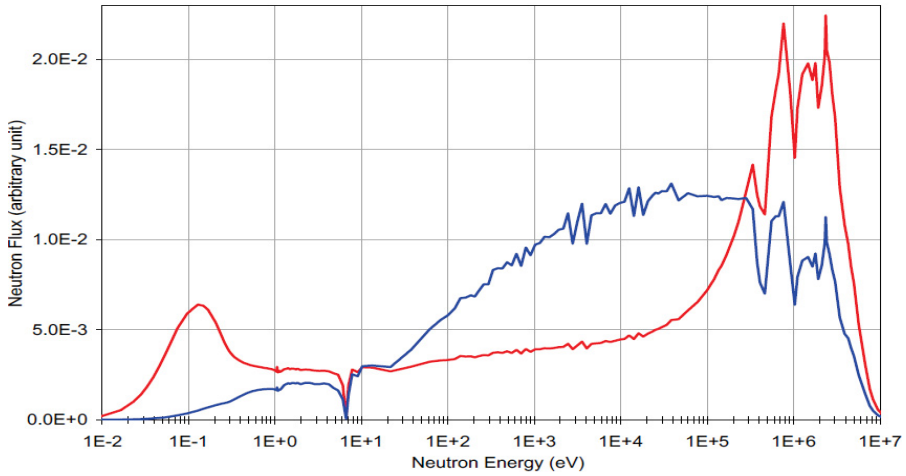

Figure 1. Neutron flux as a function of energy in a standard 4% enriched UO_2 PWR lattice (red) as well as in the same lattice but with D_2O instead of H_2O (blue).

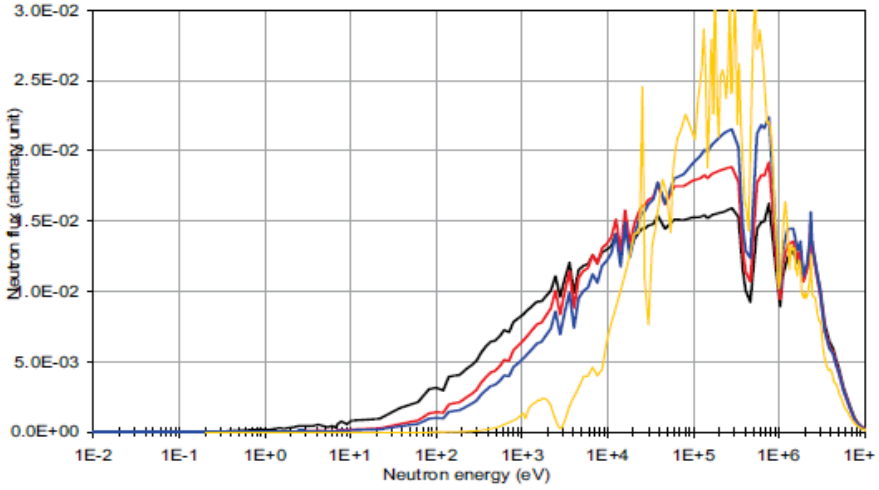

Figure 2. Neutron flux as a function of energy and for D_2O-to-fuel volume ratios of 2 (black), 1 (red) and 0.6 (blue). Sodium cooled fast reactor (orange).

2. Modeling and Calculation Method

In order to study the physics of D_2O cooled HCPWR, the burnup calculations have been performed using a set of 3D-hexagonal fuel pin-cell models, which are reasonable for evaluating the performance of axial blankets. The reflective boundary condition is applied to all six radial surfaces, while vacuum boundary condition is applied to top and bottom surfaces. The core is axially surrounded by 20cm-thick D_2O shield. We have considered water-to-fuel volume ratios of 0.45, 0.6 and 1.0 while the fuel pin diameter and stainless steel (SS) clad thickness are kept as 0.836 cm and 0.057cm, respectively. The temperature of the fuel is set to 1123.15 °K, and that of other regions (SS clad, D_2O coolant and shield) is set to 580.15 °K. The axial and internal blanket dimensions are kept as the same as those of driver fuel. The only difference from the driver fuel zone is the blanket temperature, which is set to 823.15 °K. We consider several variations in the axial length of the driver fuel and blanket while the length of the driver fuel is kept short (~75cm) in order to increase the axial neutron leakage.

We have utilized TRITON module in SCALE6.1 [9] in order to perform Monte Carlo based burnup calculations. TRITON module effectively couples KENO-VI multigroup (238-group ENDF/V-II.0) Monte Carlo calculations with ORIGEN depletion calculations. A steady state Monte Carlo calculation at each time step simulates 3000 generations with 2500 neutrons per generation, and the first 500 generations are skipped. This parameter setting is sufficient to reach the k_{eff} statistical error of around 20 pcm. The core average specific power has been set to 37 W/g over the drive fuel, corresponding to that of standard PWRs, which could reach the average discharge burnup of 51 GWd/t by Equivalent Full Power Days (EFPD) of 1351 days. Assuming a 3-batch core management scheme, the average end of cycle (EOC) burnup, B_{EOC}, is then equal to 34 GWd/t. Thus, the reactor must be critical at B_{EOC} in order to have enough reactivity to reach the target burnup of 51 GWd/t. the calculations have shown that the difference in k_{eff}'s between 3-D pin-cell and *R-Z* calculations is approximately equal to 1500 pcm based on the reference core volume of 7.5 m^3. Therefore, the fissile enrichments of all cases have been adjusted in order to have k_{eff} of 3D pin-cell calculations equal to around 1.015 at B_{EOC}.

In order to evaluate the Pu or ^{233}U conversion in D_2O-cooled HCPWR, we define the relative fissile mass balance, ΔPu_f for U-Pu core and $\Delta^{233}U$ which is the relative difference between the final and initial fissile (i.e., ^{239}Pu+^{241}Pu or ^{233}U) masses given by:

$$\Delta \text{Pu}_f \ \ or \ \Delta^{233}\text{U} = \frac{M_{Fissile}(51\ GWd/t) - M_{Fissile}(BOL)}{M_{Fissile}(BOL)} \times 100\ [\%]. \quad (1)$$

This value should be positive when the conversion ratio is more than one. The void reactivity coefficients at selected burnup points are evaluated by transferring 230-250 nuclides in each burnup zone to steady-state reference and voided 3D pin-cell models and calculate:

$$\Delta\rho = \frac{k_{eff}^{voided} - k_{eff}^{reference}}{k_{eff}^{voided} k_{eff}^{reference}} \times 10^5\ [\text{pcm}]. \quad (2)$$

Since in Eq. (2), each k_{eff} has a statistical error from KENO-VI Monte Carlo calculations, the void coefficient also contains the statistical error. Therefore, the statistical error of the void coefficients can be obtained by the error propagation:

$$\sigma_{\Delta\rho} = 10^5 \sqrt{\frac{\sigma^2_{k_{eff}^{voided}}}{k_{eff}^{voided\ 4}} + \frac{\sigma^2_{k_{eff}^{reference}}}{k_{eff}^{reference\ 4}}}\ . \quad (3)$$

3. Analyses of U-Pu Fueled Cores

3.1 Performance of Axial and Internal Blankets

The isotopic composition of MOX is shown in Table 1, and selected driver core sizes are summarized in Table 2. The last case "Core Na" has the same size as Core 5, but D_2O coolant is replaced with sodium in order to see difference in its performance from sodium cooled case. Taking driver cores in Table 2 as basis, several models are created with the blanket in which axial size varies from 4 to 30 cm. We refer the blanket positioned at the top and bottom of each driver core as an "**axial**" blanket, and the one located in the middle of core (sandwiched by two separate driver cores) as an "**internal**" blanket.

Table 1. Isotopic Composition of the MOX Fuel.

Isotopes	Pu [wt% of Pu]	Depleted U [wt% of U]
^{238}Pu	2.6	–
^{239}Pu	54.3	–
^{240}Pu	25.9	–
^{241}Pu	8.7	–
^{242}Pu	7.62	–
^{241}Am	0.88	–
^{235}U	–	0.25
^{238}U	–	99.75

Table 2. D2O-HCPWR driver core configurations.

Case	Core Height [cm]	Coolant-to-Fuel Ratio (W/F)	P/D
Core 1	72.6	1.0	1.26854
Core 2	72.6	0.6	1.15251
Core 3	72.6	0.45	1.10586
Core 4	66.4	0.45	1.10586
Core 5	60.0	0.45	1.10586
Core Na	60.0	0.45	1.10586

Table 3 presents the relative fissile Pu mass balances, ΔPu_f, for cores with the axial blanket, along with their initial Pu enrichments, as a function of blanket length. The same set of results for cores with the internal blanket is shown in Table 4. Nearly break-even cores can be attained by adding 16 cm of the axial blanket in Cores 3-5, which have the smallest W/F ratio (0.45). (Note that positive mass balances are shaded by yellow.) Core 2 can also have the positive mass balance; however, it needs much larger blanket (~30cm). The sodium cooled core (Core Na) has near break-even condition with only 4 cm of the axial blanket. However, the results are still promising that even D_2O cooled core can achieve high Pu conversion with larger blanket. On the other hand, the addition of the internal blanket is less effective than the axial one. None of configuration has shown the positive mass balance, except for Core Na, which has the positive mass balance with more than 20 cm of internal blanket. The initial Pu enrichment is strongly sensitive to the presence of the internal blanket while it is almost invariant with the addition of the axial blanket. The presence of the internal blanket promotes the axial neutron leakage and decoupling of cores. Thus, it is necessary to increase the enrichment of the core in order to compensate the loss of reactivity due to the axial leakage.

Table 3. Relative fissile Pu mass balance and initial Pu enrichment for D_2O-HCPWR with axial blanket. (Yellowed cells indicate positive Pu mass balance)

ΔPu_f [%]						
Blanket [cm]	0	4	8	16	20	30
Core 1	-12.0	-10.9	-9.7	-7.9	-7.1	-5.3
Core 2	-8.1	-6.6	-5.1	-2.6	-1.5	1.1
Core 3	-5.8	-4.0	-2.5	0.05	1.4	4.0
Core 4	-6.8	-4.9	-3.2	-0.3	1.1	4.0
Core 5	-7.6	-5.6	-3.5	-0.5	1.0	3.9
Core Na	-2.7	-0.01	2.5	7.1	9.3	14.0
Initial Pu Enrichment [wt%]						
Blanket [cm]	0	4	8	16	20	30
Core 1	20.59	20.73	20.87	21.00	21.03	21.06
Core 2	18.42	18.55	18.57	18.51	18.45	18.29
Core 3	17.40	17.53	17.55	17.55	17.47	17.36
Core 4	17.76	17.92	17.96	17.93	17.87	17.74
Core 5	18.03	18.24	18.21	18.28	18.23	18.23
Core Na	16.56	16.16	15.90	15.59	15.48	15.34

Table 4. Relative fissile Pu mass balance and initial Pu enrichment for D_2O-HCPWR with internal blanket. (Yellowed cells indicate positive Pu mass balance)

ΔPu_f [%]						
Blanket [cm]	0	4	8	16	20	30
Core 1	-12.0	-11.9	-11.1	-10.1	-9.6	-8.6
Core 2	-8.1	-8.1	-7.5	-6.6	-6.0	-5.7
Core 3	-5.8	-5.8	-5.4	-4.5	-4.0	-3.0
Core 4	-6.8	-6.7	-6.0	-5.1	-4.5	-3.6
Core 5	-7.6	-7.3	-6.5	-5.5	-4.9	-4.3
Core Na	-2.7	-2.3	-0.2	-0.2	0.4	1.7
Initial Pu Enrichment [wt%]						
Blanket [cm]	0	4	8	16	20	30
Core 1	20.59	21.93	23.13	25.08	25.67	26.24
Core 2	18.42	19.62	20.64	22.25	22.67	23.77
Core 3	17.40	18.53	19.54	20.97	21.35	21.88
Core 4	17.76	18.96	20.02	21.67	22.10	22.86
Core 5	18.03	19.32	20.62	22.36	22.92	24.14
Core Na	16.56	17.65	18.76	20.74	21.52	22.90

Figures 3a and 3b show void coefficients at 0 and 51 GWd/t as a function of the axial blanket length. As seen in these plots, the void coefficient is very sensitive to the presence of the axial blanket mainly due to the increase in the axial height of the core. Initially the addition of only 4 cm of axial blanket costs nearly 3000-4000 pcm of void coefficient in the positive direction. As a result, the void coefficient is

barely negative with the presence of the axial blanket. Moreover, by comparing Figures 3a and 3b, one can realize that the void coefficient is highly dependent on the burnup. It increases as burnup proceeds. On the other hand, the void coefficient of Core Na is almost invariant with the burnup and is negative within the presented range of axial blanket sizes. The similar dependency of the void coefficient on the burnup has been observed for cores with the internal blanket as seen in Figures 4a and 4b. The large size of the internal blanket (more than 10 cm) has an ability to decrease the void coefficient. Therefore, the combination of internal and axial blankets could be effective for the void coefficient reduction. However, it is important to note that the inclusion of the internal blanket itself introduces decoupling of the axial core power profile, which could produce high local power peaking and unstable transient.

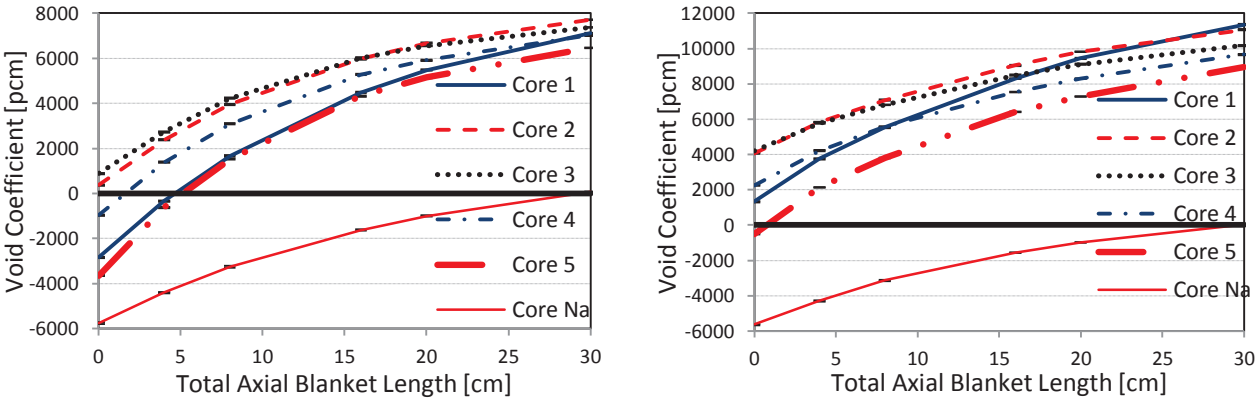

Figure 3. Void coefficient as a function of axial blanket length. (error bar=±1σ)

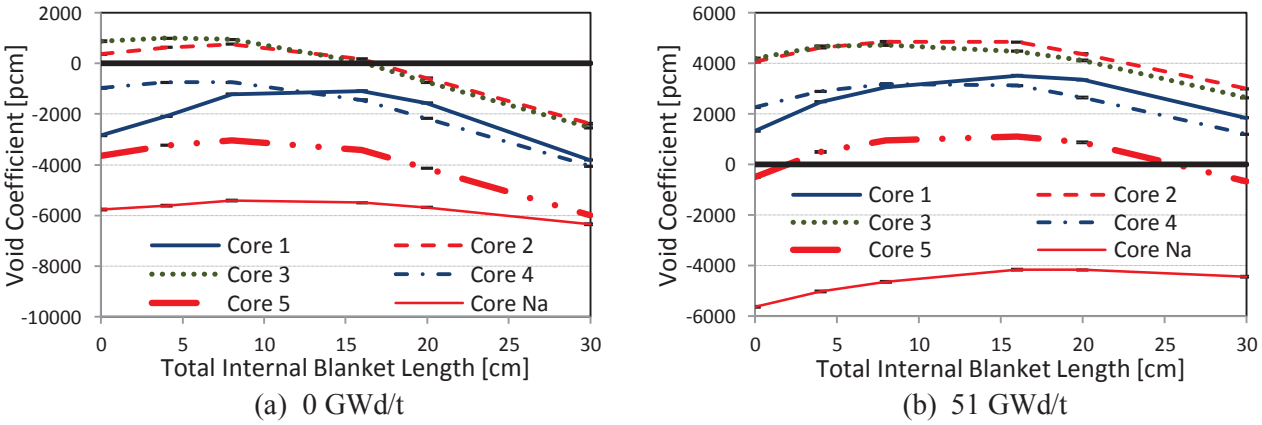

Figure 4. Void coefficient as a function of internal blanket length. (error bar=±1σ)

One may obtain more effective Pu conversion by reducing the coolant density in order to further harden the neutron spectrum. Such a condition could be attained by boiling D_2O coolant in the reactor core. The realistic design of high conversion BWR is highly thermal-hydraulic dependent and axially asymmetric[3]. In this analysis, we perform simple study, without considering thermal-hydraulic feedback, by uniformly reducing the coolant density according to the voiding factor to see the rough average Pu breeding performance of boiling D_2O reactor. (Note that if the voiding factor is x×100%, then the D_2O density is multiplied by (1-x).) Table 5 shows the relative fissile Pu mass balance and initial Pu enrichment as a function of the voiding factor of the coolant with various axial blanket sizes. (The axial blanket length is shown within the parenthesis next to the core name.) If the core has the positive void

coefficient at B_{EOC}, then the initial Pu enrichment has to be decreased in order to preserve the reactivity, and vice versa. As a result, Cores 2 and 5 with 4 cm of blanket, which have a positive void coefficient at B_{EOC}, have less enrichment when the coolant density is reduced. Core 2 also has a positive void coefficient at the beginning of the cycle (BOC). This results in significant reduction of Pu enrichment and improvement in the mass balance. The reduction of the coolant density reduces the magnitude of the void coefficient but does not change the sign of it (see Figure 5). Therefore, despite the improvement in the Pu mass balance, Core 2 may not the preferable option. The results of Core 5 show some promising signs. It has a negative void coefficient until B_{EOC} (except for the one with 4 cm of blanket), and ~1.8% increase in the Pu mass balance can be observed with 40-60% of the voiding factor.

Table 5. ΔPu_f and initial Pu enrichment for boiling D_2O reactor as a function of the voiding factor.

ΔPu_f [%]						
Voiding Factor [%]	0	40	50	60	70	80
Core 2 (4 cm)	-6.6	-3.1	-2.5	-1.8	-1.5	-1.4
Core 5 (0 cm)	-7.6	-6.1	-6.0	-6.0	-6.1	-6.5
Core 5 (2 cm)	-6.5	-4.9	-4.8	-4.8	-5.0	-5.4
Core 5 (4 cm)	-5.6	-3.9	-3.8	-3.7	-3.9	-4.4
Initial Pu Enrichment [wt%]						
Voiding Factor [%]	0	40	50	60	70	80
Core 2 (4 cm)	18.55	17.52	17.35	17.18	16.98	16.80
Core 5 (0 cm)	18.03	18.21	18.34	18.40	18.54	18.65
Core 5 (2 cm)	18.11	18.10	18.18	18.20	18.28	18.33
Core 5 (4 cm)	18.24	18.04	18.09	18.05	18.08	18.07

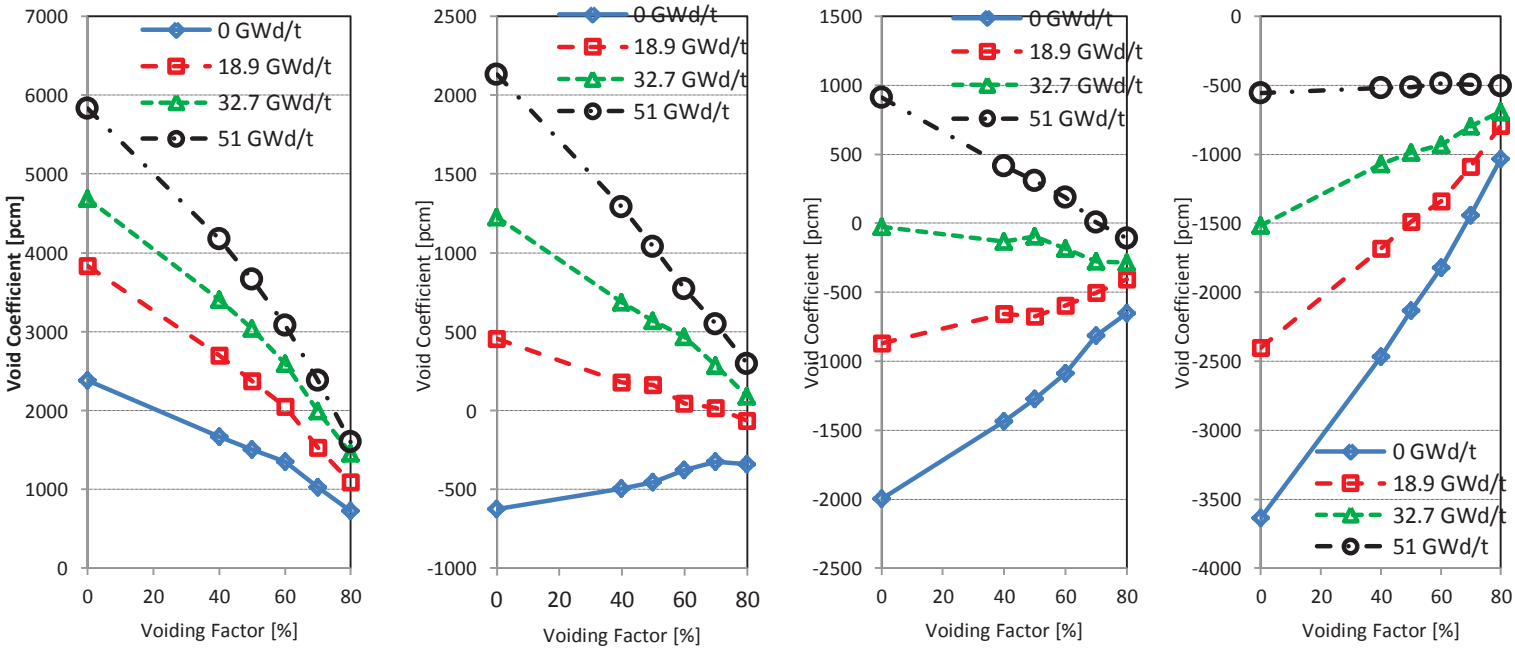

(a) Core 2 (4 cm) (b) Core 5 (4 cm) (c) Core 5 (2 cm) (d) Core 5 (0 cm)

Figure 5. Void coefficient as a function of voiding factors.

The conclusion in this section is that based on our analysis, it seems to be difficult, if not impossible, to obtain break-even or near breeding MOX fueled D_2O-HCPWR utilizing only axial or internal blanket while retaining the negative void coefficient. It is necessary to have radial blankets to achieve higher Pu conversion. Also the optimum core design could be highly heterogeneous in both radial and axial directions in order to increase the neutron leakage, and as such cannot be determined by simple fuel pin-cell or assembly models.

3.2 MOX Fuel with Different U235 Enrichments

The analyses shown so far in this report have been carried out the MOX fuel with the composition given in Table 1 which is based on the tail uranium (0.25 wt% ^{235}U and 99.75 wt% ^{238}U). One of reasons that the selected core configurations could not attain the break-even condition while retaining the negative void coefficient is the high initial Pu content required to reach the target burnup. The initial Pu content can be reduced by utilizing enriched uranium in order to compensate the reactivity. This section will study the effect of MOX fuel with different ^{235}U enrichment on the Pu conversion performance of D_2O cooled HCPWRs.

Figure 6 shows the characteristics of Pu conversion as a function of ^{235}U enrichment in MOX fuel studied by the core with 60 cm of height (without blanket) and W/F ratio of 0.45. The Pu enrichment decreases as increasing the ^{235}U enrichment, and nearly 40% of ^{235}U, regardless of its enrichment, is utilized by the end of the cycle. The break-even condition can be attained with around 3.5 wt% of ^{235}U enrichment. The use of enriched uranium increases the production of ^{236}U, which is a long-lived and nuisance radioactive waste difficult to separate while reprocessing. Assuming that the recovered uranium is used for the MOX fabrication, the presence of ^{236}U decreases the reactivity of fresh fuel because of its capture cross section. The addition of the axial blanket could help to reach the break-even condition with less enriched uranium.

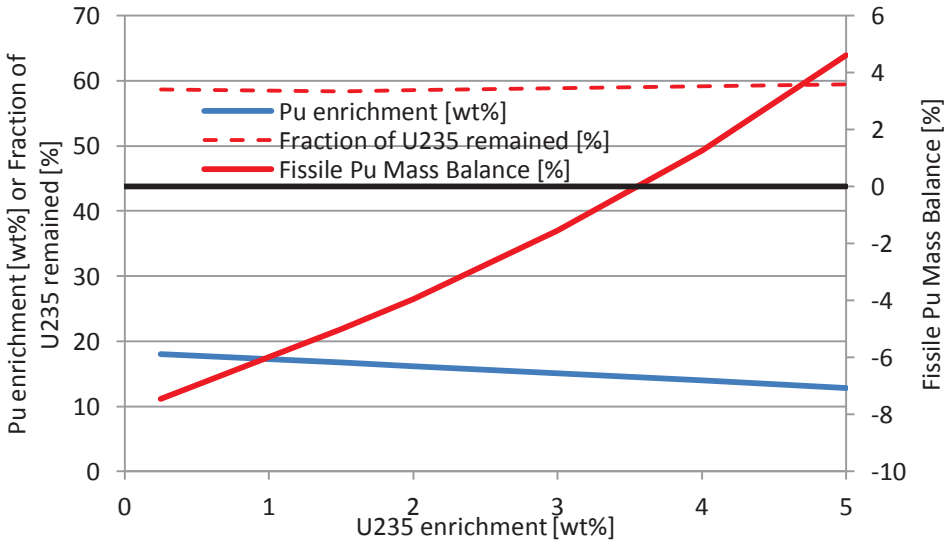

Figure 6. Pu mass balance and enrichment as a function of ^{235}U enrichment

Table 6 shows ΔPu_f and initial Pu enrichment of cores as a function of blanket sizes and ^{235}U enrichment in the MOX fuel. The positive mass balance (or breeding condition) can be observed when the ^{235}U enrichment is 2-3 wt% and axial blanket size is over 4 cm. Also the nearly breakeven condition can be achieved by 2 cm blanket with 3 wt% of ^{235}U and 8 cm blanket with 1.5 wt% of ^{235}U. Table 7 presents the void coefficient for corresponding cases shown in Table 6 as a function of burnup. ^{239}Pu has slightly higher values of η (i.e., the average number of neutrons produced per neutron absorbed) in the fast neutron energy range than ^{235}U. Thus, the void coefficient decreases as increasing ^{235}U enrichment which

reduces the Pu enrichment. None of cores with 8cm blanket shows the negative void coefficient despite the fact that those with enriched uranium reached nearly break-even or breeding conditions. Those with 2-4 cm of blanket have the negative void coefficient at the initial stage of the cycle, however, nearly 3 wt% of ^{235}U enrichment is needed in order to obtain negative void coefficient until the target burnup of 51 GWd/t. Hardening of spectrum by D_2O coolant boiling, as we presented in Section 3.1, could further reduce ^{235}U enrichment while increasing the mass balance of Pu.

Table 6. ΔPu_f and initial Pu enrichment as a function of axial blanket size and ^{235}U enrichment. (Yellowed cells indicate positive Pu mass balance)

ΔPu_f [%]				
U235 enrichment [wt%]	0.25	1.5	2	3
0 cm	-7.44%	-5.00%	-3.95%	-1.54%
2 cm	-6.14%	-3.72%	-2.54%	-0.05%
4 cm	-5.05%	-2.44%	-1.25%	1.26%
8 cm	-3.54%	-0.30%	0.92%	3.67%
Initial Pu Enrichment [wt%]				
U235 enrichment [wt%]	0.25	1.5	2	3
0 cm	18.03	16.69	16.17	15.06
2 cm	18.06	16.76	16.23	15.14
4 cm	18.08	16.77	16.24	15.16
8 cm	18.21	16.75	16.21	15.14

Table 7. Void coefficients [pcm] as a function of burnup with several blanket sizes and ^{235}U enrichment. (Yellowed cells indicate positive void coefficient)

0.25 wt% of ^{235}U				
	0 cm	2 cm	4 cm	8 cm
0 Gwd/t	-3658.32	-2048.54	-711.70	1526.15
18.9 Gwd/t	-2315.04	-825.84	419.54	2396.09
32.7 Gwd/t	-1394.91	26.34	1259.53	3054.17
51 Gwd/t	-417.22	1040.00	2157.94	3805.54
1.5 wt% of ^{235}U				
	0 cm	2 cm	4 cm	8 cm
0 Gwd/t	-4425.85	-2693.07	-1312.19	908.60
18.9 Gwd/t	-3009.12	-1459.75	-224.27	1776.01
32.7 Gwd/t	-2126.20	-614.42	520.61	2454.11
51 Gwd/t	-991.46	420.96	1569.04	3396.65
2.0 wt% of ^{235}U				
	0 cm	2 cm	4 cm	8 cm
0 Gwd/t	-4684.82	-3033.96	-1577.78	695.55
18.9 Gwd/t	-3258.49	-1724.63	-482.93	1521.65
32.7 Gwd/t	-2416.86	-904.11	256.17	2236.43
51 Gwd/t	-1351.83	89.51	1308.15	3109.90
3.0 wt% of ^{235}U				
	0 cm	2 cm	4 cm	8 cm
0 Gwd/t	-5452.50	-3620.33	-2166.92	158.33
18.9 Gwd/t	-3922.21	-2335.55	-1049.09	978.01
32.7 Gwd/t	-3003.82	-1537.32	-227.47	1723.52
51 Gwd/t	-1888.05	-319.99	817.35	2679.33

Tables 8-10 show Pu mass balance and void coefficient, along with initial Pu enrichment and final U compositions, for selected fuel pins immersed in the boiled D_2O (reduced coolant density) according to the voiding factor defined in Section 3.1. The observation here is consistent to that in Section 3.1. The maximum of Pu mass balance occurs between 40 and 60% of voiding factors showing ~1.8% increase. As increasing the voiding factor, mostly the magnitude of void coefficient becomes small without changing the sign (there are few exceptions in Tables 8 and 9) since the core approaches fully voided condition. Nevertheless the analyses have been performed utilizing simplified models, the results tells us that the boiling of D_2O coolant is the promising approach to increase the Pu conversion ratio.

Table 8. Performance of boiling D_2O core with 2 cm of blanket and 2 wt% of ^{235}U enrichment.

Voiding Factor	0.00%	40.00%	50.00%	60.00%
Pu enrichment [wt%]	16.227	16.271	16.296	16.349
Pu mass balance [%]	-2.5	-1.1	-1.0	-1.0
U235 final content [wt% of U]	1.253	1.292	1.307	1.324
U234 final content [wt% of U]	0.013	0.013	0.013	0.013
U236 final content [wt% of U]	0.222	0.202	0.195	0.187
Void coefficients [pcm]				
0GWd/t	-3034.0	-2139.9	-1867.2	-1631.9
18.9GWd/t	-1724.6	-1276.3	-1188.8	-964.0
32.7GWd/t	-904.1	-773.3	-738.6	-699.8
51.0GWd/t	89.5	-123.7	-214.4	-264.3

Table 9. Performance of boiling D_2O core with 4 cm of blanket and 2 wt% of ^{235}U enrichment.

Voiding Factor	0.00%	40.00%	50.00%	60.00%
Pu enrichment [%]	16.240	16.121	16.104	16.111
Pu mass balance [%]	-1.2	0.4	0.5	0.6
U235 final content [wt% of U]	1.254	1.290	1.303	1.319
U234 final content [wt% of U]	0.013	0.013	0.013	0.013
U236 final content [wt% of U]	0.221	0.203	0.196	0.188
Void coefficients [pcm]				
0GWd/t	-1577.8	-1157.4	-1050.0	-877.2
18.9GWd/t	-482.9	-450.3	-437.7	-340.7
32.7GWd/t	256.2	50.7	90.8	-46.9
51.0GWd/t	1308.1	694.1	506.1	412.2

Table 10. Performance of boiling D_2O core with 4 cm of blanket and 4 wt% of ^{235}U enrichment.

Voiding Factor	0.00%	40.00%	50.00%	60.00%
Pu enrichment [%]	15.157	15.124	15.134	15.164
Pu mass balance [%]	1.3	2.7	2.9	2.7
U235 final content [wt% of U]	1.895	1.950	1.969	1.993
U234 final content [wt% of U]	0.012	0.012	0.012	0.012
U236 final content [wt% of U]	0.328	0.300	0.290	0.278
Void coefficients [pcm]				
0GWd/t	-2166.9	-1521.5	-1396.4	-1195.9
18.9GWd/t	-1049.1	-818.5	-699.0	-677.4
32.7GWd/t	-227.5	-350.4	-232.1	-315.9
51.0GWd/t	817.3	395.4	268.1	81.2

3.3 Effect of Different Target Burnups on the Pu Conversion

All analyses shown so far in this report are based on the target burnup of 51 GWd/t assuming 3-batch cores. It is worthwhile to study the effect of different burnup on the conversion performance since the higher or lower target burnup may result in the better Pu conversion because of change in the irradiation mechanism. For instance, the lower burnup core requires less initial Pu content, thus it may readily reach break-even condition. On the other hand the higher burnup core improves fuel economy, however, needs more initial Pu content. For the purpose of this study, two target burnups, lower (34 GWd/t) and higher (85 GWd/t), are considered. The lower burnup core assumes 2-batch (average burnup=25.5GWd/t), and the higher burnup core assumes 5-batch (average burnup=51GWd/t).

Figures 7a and 7b show the relative fissile Pu mass balance and initial Pu enrichment as a function of target burnup for cores with various axial sizes of blanket. The relative Pu mass balance decreases as increases target burnup, and vice versa for the initial Pu enrichment. These two quantities have almost linearly related to the target burnup. Figure 8 presents void coefficients as a function of burnup for cores with different target burnups. Each vertical black bold line indicates the target burnup. The figure exhibits slight increase in the void coefficient for cores with higher target burnup, which is caused by the increase in the initial Pu enrichment. Other than this difference along with the difference caused by the addition of axial blanket, there is no vivid distinction within them, and void coefficients are almost on the same track through target burnups. In this regards, the lower target burnup could help the core to attain both high Pu conversion and negative void coefficient. However, from the fuel cycle view point, the lower target burnup increases the number of reprocessing per unit energy. Thus, it could not be the preferable and economical option considering the reprocessing loss of Pu.

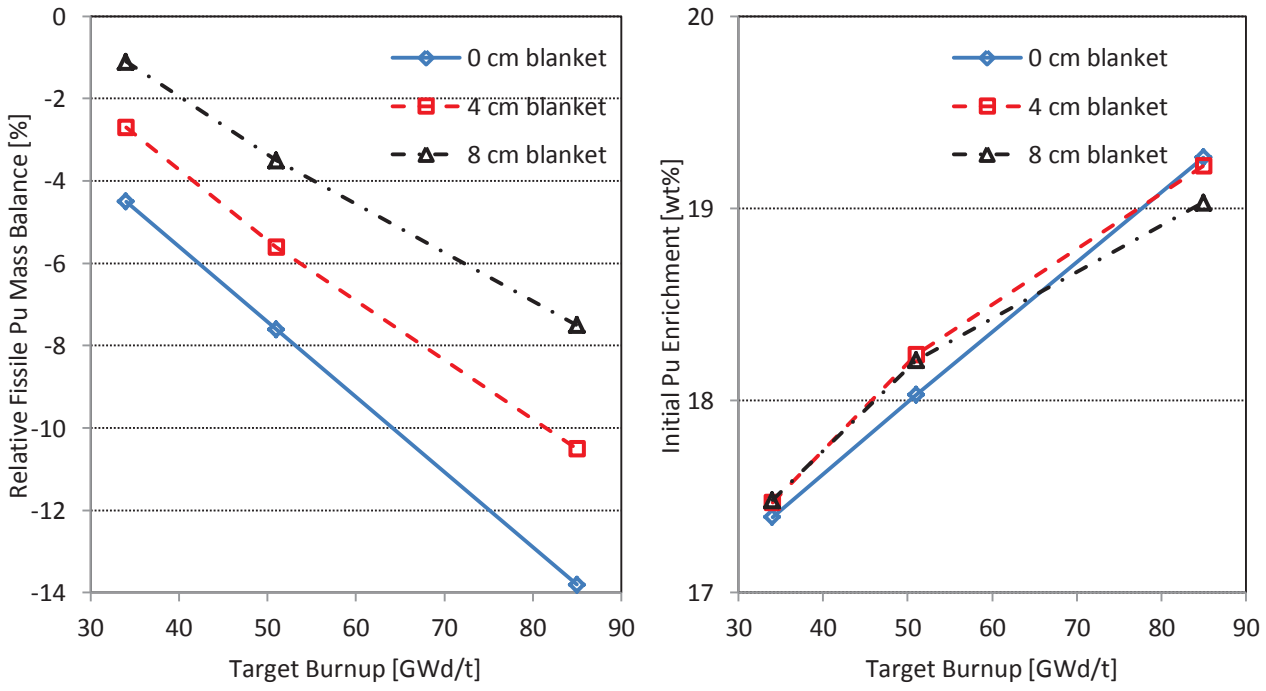

(a) Relative fissile Pu mass balance (b) Initial Pu enrichment

Figure 7. Relative fissile Pu mass balance and initial Pu enrichment as a function of target burnup.

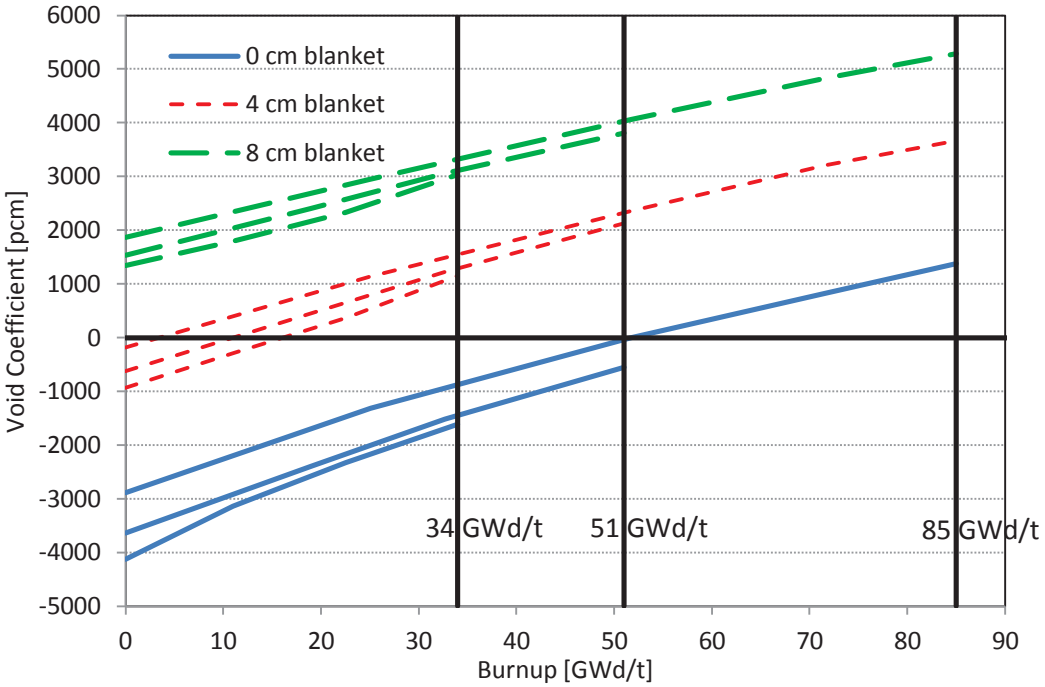

Figure 8. Void coefficients as a function of burnup.

4. Analyses of Th-U Fueled Cores

This section presents preliminary studies for Th-U fueled cores utilizing similar set of models used for MOX fueled cores studied in Section 3. The nuclide of ^{233}U produced by (n,γ) reaction on ^{232}Th has several promising characteristics over other fissile like ^{239}Pu and ^{235}U, most notably its higher fission neutrons per absorption, η, in thermal and epithermal ranges and stability (it has longer half-life (1.6×10^5 years) than ^{239}Pu (2.4×10^4 years)). In particular the former combined with lower η in the fast range than ^{239}Pu results in more significant margins in coolant voiding. This could allow to use taller cores than MOX ones while retaining the negative void reactivity. In this type of fuel cycle, however, initially there is no ^{233}U nuclide, therefore, in practice, it is necessary to introduce ^{239}Pu or ^{235}U in order to transition into full Th-U cycle. The analyses in this section assume that ^{233}U nuclides are initially available in order to estimate the performance of D_2O-cooled high-conversion PWRs.

4.1 Performance of Axial and Internal Blankets

The analyses have been started with two types of short cores (H=60 cm, W/F=0.45 or 0.6) which have shown the most promising performance in terms of both Pu conversion and void reactivity for the MOX fueled case. The blanket is accumulated until its total axial length reaches 60cm. Tables 11 shows the relative ^{233}U mass balance and the initial ^{233}U enrichment as a function of axial blanket lengths. The same counterpart for the internal blanket is shown in Table 12. The void coefficients as a function of axial blanket lengths at 0 and 51 GWd/t are plotted in Figures 9a and 9b, respectively. As observed in the MOX fueled core, the axial blanket outperforms the internal blanket for ^{233}U mass balance. Nearly 6% of increase in mass balance can be attained by adding of 60 cm blanket. The void coefficients of both cores are much lower than those of MOX fueled cores and retain negative values until the target burnup of 51 GWd/t even with around 40 cm of blanket. However, it could not achieve either break-even condition or positive mass balance. In this respect, the utilization of driver cores taller than 60 cm could help to reach the higher ^{233}U conversion while still keeping the negativity in the void coefficient. The addition of the

internal blanket seems to be ineffective such that it reduces ^{233}U mass balance while it also decreases the void coefficient with more than 20 cm of internal blanket.

Table 11. Relative ^{233}U mass balance and initial ^{233}U enrichment for 60cm-driver cores with axial blanket.

$\Delta^{233}U_f$ [%]									
Blanket [cm]	0	2	4	10	20	30	40	50	60
60cm, W/F=0.45	-11.2	-10.6	-10.2	-8.9	-7.6	-6.7	-6.0	-5.5	-5.3
60cm, W/F=0.6	-11.9	-11.4	-10.9	-9.8	-8.6	-7.7	-7.1	-6.7	-6.5
Initial ^{233}U Enrichment [wt%]									
Blanket [cm]	0	2	4	10	20	30	40	50	60
60cm, W/F=0.45	11.37	11.66	11.90	12.24	12.37	12.39	12.40	12.43	12.45
60cm, W/F=0.6	11.37	11.69	11.94	12.31	12.48	12.52	12.53	12.55	12.58

Table 12. Relative ^{233}U mass balance and initial ^{233}U enrichment for 60cm-driver cores with internal blanket.

$\Delta^{233}U_f$ [%]									
Blanket [cm]	0	2	4	10	20	30	40	50	60
60cm, W/F=0.45	-11.2	-11.5	-12.0	-13.5	-14.3	-14.3	-13.9	-13.6	-13.3
60cm, W/F=0.6	-11.9	-12.2	-12.7	-14.1	-14.9	-14.8	-14.5	-14.2	-13.9
Initial ^{233}U Enrichment [wt%]									
Blanket [cm]	0	2	4	10	20	30	40	50	60
60cm, W/F=0.45	11.37	11.76	12.18	14.03	15.29	15.89	15.78	15.73	15.58
60cm, W/F=0.6	11.37	11.74	12.16	14.06	15.27	16.03	15.99	15.85	15.74

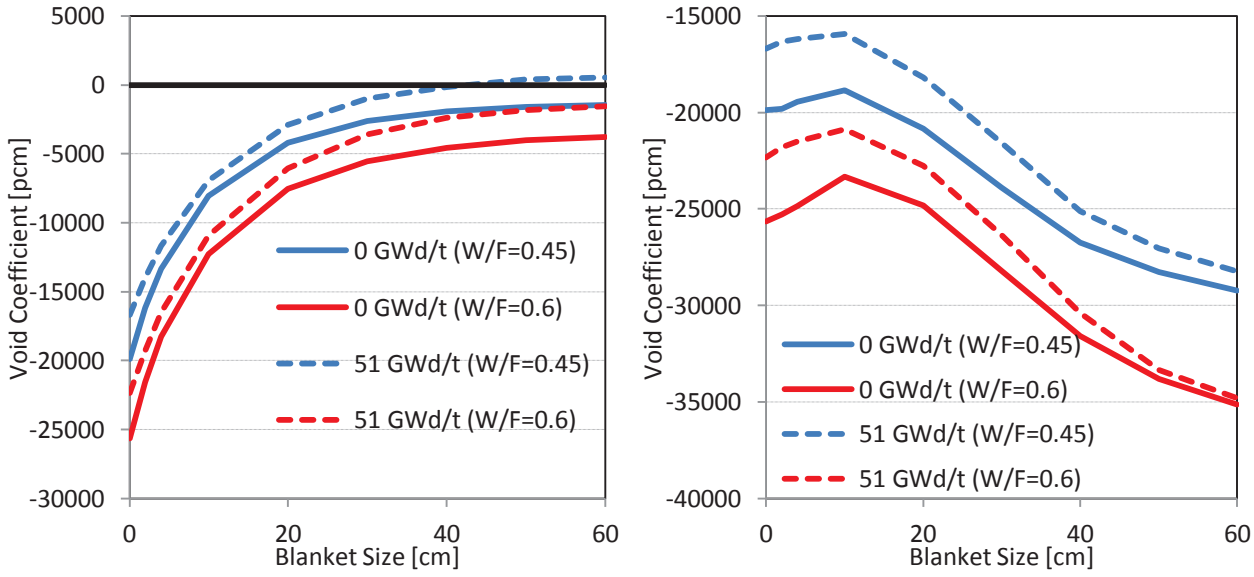

(a) Axial Blanket (b) Internal Blanket

Figure 9. Void coefficients of 60cm-driver cores as a function of axial length of the blanket. (stdev≅30pcm)

Total of five cores (named as Cores A-E) with the taller driver zone have been selected. The size of driver zones ranges from 80 to 120 cm, and their W/F ratio is either 0.45 or 0.6. Table 13 presents the relative mass balance and initial enrichment of ^{233}U as a function of axial blanket lengths, and Figure 10 shows the void coefficients at 0 and 51 GWd/t as a function of blanket length. Cores C and E are able to reach near break-even condition with 60 cm of blanket. However, void coefficients of these cores become positive at the target burnup of 51 GWd/t. Based on our analyses, the maximum fissile mass balance while retaining the negative void reactivity until the target burnup is around -3.5% which is much higher than the MOX cores (-7.6%) in our investigation.

Table 13. Relative ^{233}U mass balance and initial ^{233}U enrichment for taller cores with axial blanket.

$\Delta^{233}U_f$ [%]						
Blanket [cm]	0	4	10	20	40	60
Core A, 80cm, W/F=0.45	-7.4	-6.4	-5.5	-4.3	-2.9	-2.2
Core B, 80cm, W/F=0.6	-8.4	-7.6	-6.6	-5.5	-4.2	-3.7
Core C, 100cm, W/F=0.45	-4.8	-3.9	-3.1	-2.1	-1.0	-0.4
Core D, 100cm, W/F=0.6	-5.9	-5.1	-4.2	-3.4	-2.4	-1.8
Core E, 120cm, W/F=0.6	-4.1	-3.4	-2.7	-1.9	-1.2	-0.8
Initial ^{233}U Enrichment [wt%]						
Blanket [cm]	0	4	10	20	40	60
Core A, 80cm, W/F=0.45	10.49	10.81	10.99	11.02	11.01	11.01
Core B, 80cm, W/F=0.6	10.55	10.87	11.06	11.10	11.09	11.08
Core C, 100cm, W/F=0.45	10.03	10.23	10.35	10.36	10.35	10.34
Core D, 100cm, W/F=0.6	10.05	10.26	10.37	10.40	10.41	10.37
Core E, 120cm, W/F=0.6	9.75	9.91	9.98	10.00	10.00	10.00

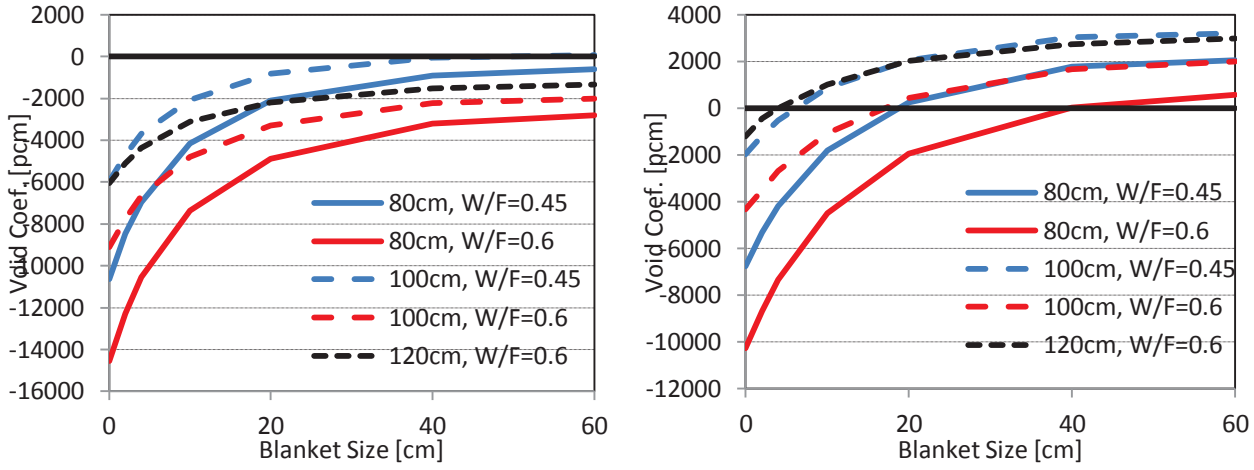

(a) At BOL (b) At 51 GWd/t

Figure 10. Void coefficients of taller cores as a function of axial blanket length. (stdev≅30pcm)

4.2 Comparison of U-Pu and Th-U Cores

The analyses for selected core configurations performed in Sections 3 and 4 can visually represent difference in the conversion performance of U-Pu and Th-U cores. Comparisons can be made more in detail by defining the quantity expressing the change in the quantity of interest (e.g., mass balance, void coefficient, k_{eff}) relative to the small change in the other parameter (e.g., enrichment), which is similar to the sensitivity coefficient. For this comparison, we have defined following three quantities:

$\frac{M_{fissile}}{k_{eff}^{34GWd}} \frac{\partial k_{eff}^{34GWd}}{\partial M_{fissile}}$ – k_{eff} sensitivity at the average burnup of 34GWd/t relative to the change in the initial fissile content. (Coefficient A),

$\frac{k_{eff}^{34GWd}}{\Delta Pu_f} \frac{\partial \Delta Pu_f}{\partial k_{eff}^{34GWd}}$ – Fissile mass balance sensitivity relative to the change in k_{eff} at the average burnup of 34 GWd/t (Coefficient B), and

$\frac{k_{eff}^{34GWd}}{\Delta \rho} \frac{\partial \Delta \rho}{\partial k_{eff}^{34GWd}}$ – Void coefficient sensitivity relative to the change in k_{eff} at the average burnup of 34 GWd/t (Coefficient C).

All derivatives are approximated by the forward difference between two quantities that result in k_{eff}^{34GWd} of around 1.015 and 1.005, for instance:

$$\frac{\partial \Delta Pu_f}{\partial k_{eff}^{34GWd}} \cong \frac{\Delta Pu_f\left(k_{eff}^{34GWd} \cong 1.015\right) - \Delta Pu_f\left(k_{eff}^{34GWd} \cong 1.005\right)}{k_{eff}^{34GWd}(\cong 1.015) - k_{eff}^{34GWd}(\cong 1.005)} \quad . \tag{4}$$

Note that the perturbation of k_{eff} at the average burnup of 34 GWd/t implies perturbations of the radial neutron leakage and/or radial dimension and initial Pu content.

All comparisons have been made for cores having 60 cm of driver fuel zone and W/F ratio of 0.45. Figures 11a and 11b show the plots of Coefficients A and B, respectively, for Th-U and U-Pu fueled cores as a function of axial blanket length. Coefficient A for each core is positive, however, that of Th-U core is slightly higher than U-Pu core. This possibly indicates that the reactivity swing of Th-U core is slightly smaller than that of the U-Pu core. Coefficients B of both cores are negative, which means the increase in the initial fissile enrichment gives a rise to the reduction of fissile mass balance. The figure indicates that this effect is much larger for U-Pu core in particular with large axial blanket. Figures 12a and 12b present Coefficients C for Th-U and U-Pu cores, respectively. Both plots show that Coefficient C is always positive. It explains that the increase in initial fissile content results in the increase in the void coefficient. This coefficient is also higher for U-Pu core than Th-U core. These simple comparisons have also proved that Th-U cycle is the promising way to improve the conversion ratio with lower void coefficient.

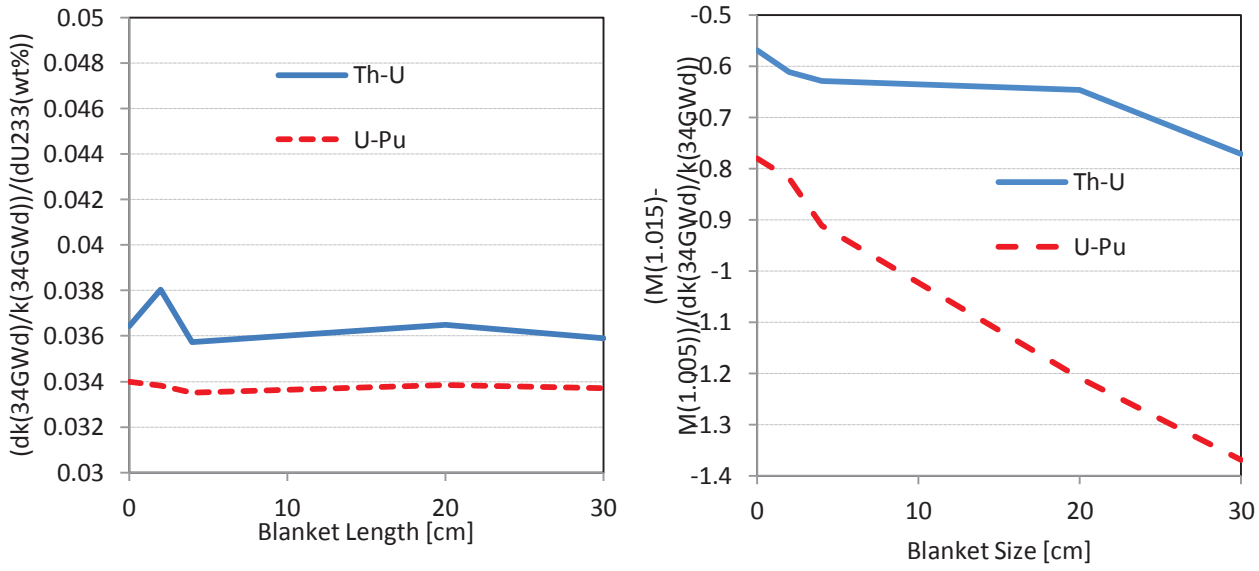

(a) $\frac{M_{fissile}}{k_{eff}^{34GWd}} \frac{\partial k_{eff}^{34GWd}}{\partial M_{fissile}}$ (b) $\frac{k_{eff}^{34GWd}}{\Delta Pu_f} \frac{\partial \Delta Pu_f}{\partial k_{eff}^{34GWd}}$

Figure 11. Comparisons of Coefficients A and B between Th-U and U-Pu cores.

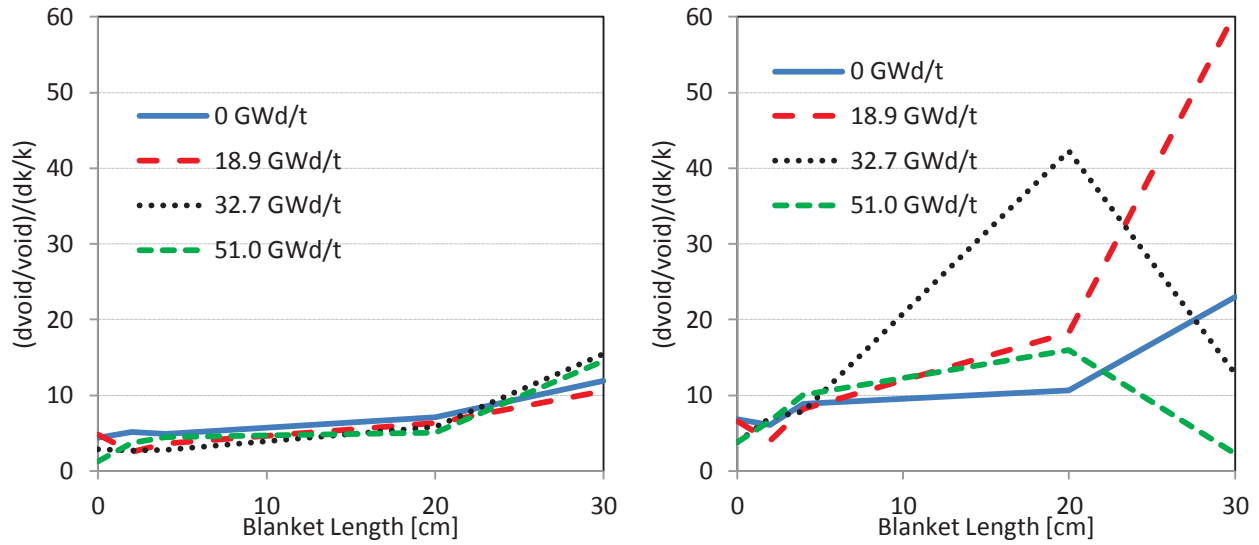

(a) Th-U Core (b) U-Pu Core

Figure 12. Comparisons of Coefficient C between Th-U and U-Pu cores.

5. Study of the Effect of Advanced Iron Alloy Cladding on the Pu Conversion Performance in D_2O-Cooled HCPWRs

There has recently been growing interest in the application of the advanced oxidation resistant iron-based alloys, instead of zirconium alloy, as light-water reactor fuel cladding that could have improved accident tolerance [10]. It is expected that in the thermal neutron reactors there is a neutronic penalty upon the transition from zirconium alloy to iron based alloy cladding because of the increase in the thermal neutron absorption. However, in the fast neutron high-conversion reactors, utilizing the advanced iron based alloy (e.g., FeCrAl, see Table 14) instead of the stainless steel cladding could have advantage in the neutronic mechanism without losing the mechanical strength in a sense that it is more transparent to the neutron than SS cladding because of the absence of nickel. Thus, it is of great interest to evaluate the Pu conversion performance of D_2O-cooled HCPWRs with such advanced alloys.

The reference model of this analysis is the core with 60cm-driver zone and 4cm of axial blanket having W/F ratio of 0.45. Upon utilizing two types of cladding materials shown in Table 14, several variants in the model have been considered. The first case is the reference configuration that has clad thickness of 0.57mm. The second variant reduces the clad thickness to 0.4mm. This will automatically increase D_2O coolant volume and result in W/F ratio of 0.54. The third case tightens the fuel pin-pitch of the second case and reduces the W/F ratio to the original value of 0.45. The target burnup of all cases is set to 51 GWd/t assuming 3-batch core. Thus, the Pu enrichment is adjusted to have k_{eff} of 1.015 at the average burnup of 34 GWd/t, as explained in Section 2.

Table 14. Cladding material composition (in wt%).

Element	Stainless Steel	FeCrAl
Fe	74.57	75
Cr	12.28	20
Ni	9.74	–
Al	–	5
Mn	1.12	–
Mo	1.32	–
Ti	0.25	–
Si	0.72	–

Figure 13 shows the evolution of k_{eff} as a function of burnup for models with SS and FeCrAl claddings having different thicknesses and coolant volumes, and Table 15 presents Pu mass balance and enrichment of each case. The type of cladding has only minor contribution to the difference in k_{eff} evolutions; however, the clad thickness has some impacts on it. Those having smaller clad thickness (i.e., 0.4mm) with larger D_2O coolant volume (i.e., W/F=0.54) have larger reactivity swing than others. There is slight reduction in the Pu enrichment upon transition from reference to thinner clad because of the reduction in the neutron absorption rate; however, there is also reduction in the Pu mass balance since a part of cladding is now replaced with D_2O coolant, thus the slightly softer spectrum is expected. Tightening the pin-pitch to reset the W/F ratio as the original value of 0.45 further reduces the Pu enrichment due to the increase in Pu mass in the core and significantly increases in the Pu mass balance because of the spectrum hardening. The use of FeCrAl instead of SS as a cladding alloy reduces the required Pu enrichment and improves the Pu conversion rate. This difference is primarily due to the absence of nickel in the cladding alloy that results in the reduction of the neutron absorption. Figure 14 shows void coefficients of all cases as a function of burnup. Void coefficients of thin cladding are initially over 500 pcm less than those of reference ones and gradually approach to them as burnup proceeds. The difference in void coefficients between SS and FeCrAl alloys is nearly 500 pcm over the entire burnup

range, which clearly indicates that the neutron absorption caused by the presence of nickel in SS cladding significantly affects the void coefficient.

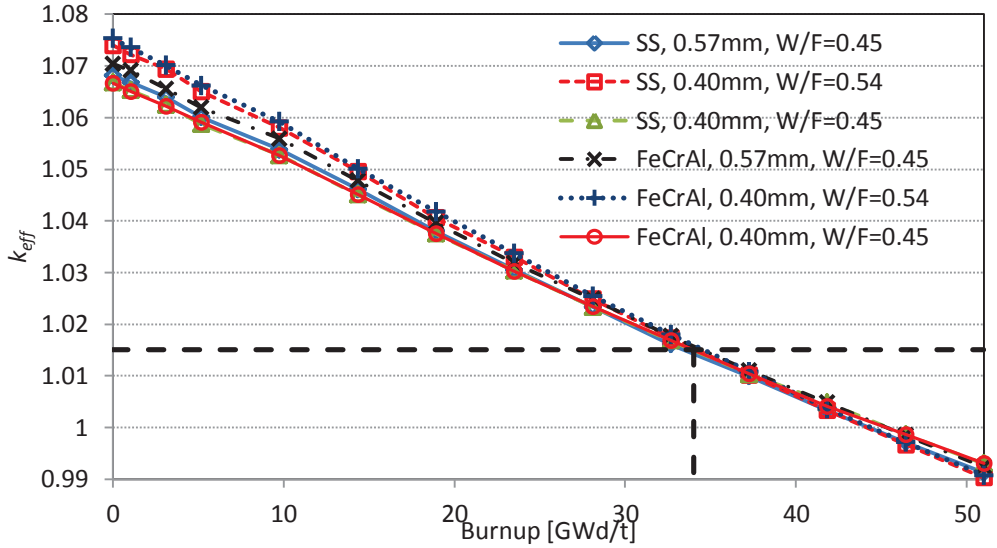

Figure 13. k_{eff} evolution of 3D-pin cell models until 51 GWd/t with SS and FeCrAl claddings having different thicknesses and water-to-fuel volume ratios. (stdev≅20pcm)

Table 15. Pu mass balance and initial enrichment of 3D-pin cell models with SS and FeCrAl claddings.

Clad Type	Pu Mass Balance [%]	Initial Pu Enrichment [wt%]
SS, 0.57mm, W/F=0.45	1.26	15.157
SS, 0.40mm, W/F=0.54	0.71	15.094
SS, 0.40mm, W/F=0.45	3.44	14.305
FeCrAl, 0.57mm, W/F=0.45	1.58	14.991
FeCrAl, 0.40mm, W/F=0.54	0.94	14.943
FeCrAl, 0.40mm, W/F=0.45	3.90	14.131

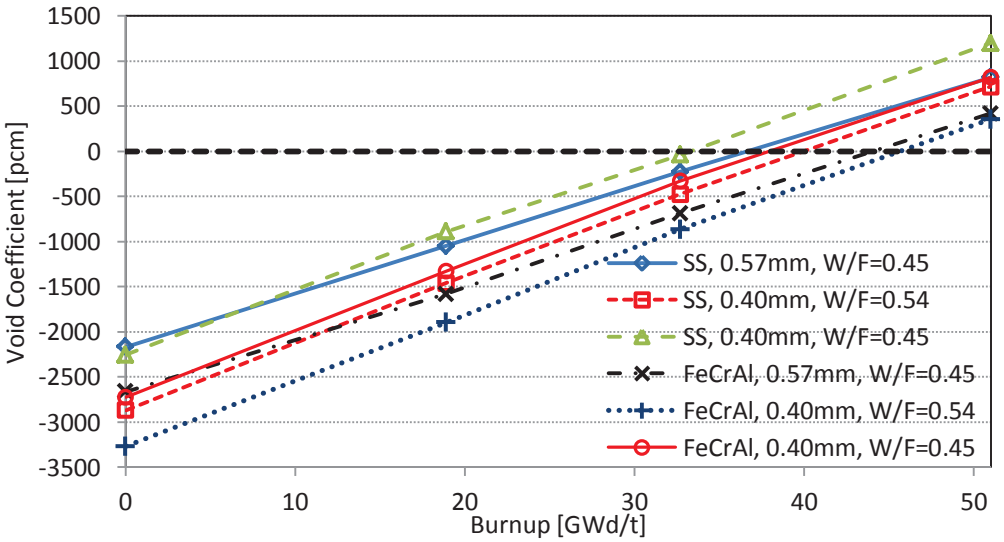

Figure 14. Void coefficients [pcm] of 3D-pin cell models until 51 GWd/t with SS and FeCrAl claddings having different thicknesses and water-to-fuel volume ratios. (stdv≅30pcm)

6. Application to Fuel Cycle Calculations

This section demonstrates the simulation of the U-Pu fuel-cycle based on D_2O cooled HCPWR core. In this study, we assume the fresh Pu shown in Table 16 recovered from SFR blanket is mixed with depleted uranium for MOX fabrication, and the fabricated MOX fuel is rest for 2 years. Then, the fuel is used for D_2O-HCPWR until the target burnup of 50 GWd/t. At the end of each cycle followed by 5 years of cooling, Pu is recycled back into the reactor with fresh Pu topping necessary to reach the target burnup of 50 GWd/t. This process is repeated until the core reaches equilibrium. No recycle loss of Pu is considered. The reference full core is set to have a core volume of 7.5 m^3 with a water-to-fuel volume ratio of 0.45 and core height-to-diameter ratio of 0.15. The core average specific power has been set to 37 W/g, which could reach the average discharge burnup of 50 GWd/t by Equivalent Full Power Days (EFPD) of 1351 days. The 3D fuel-pin cell model was used for the burnup calculations. The model considered here has an active core height of 60 cm and W/F ratio of 0.45, which has a capability to reach the relative Pu mass balance of -7.6% (see Table 3). The fuel-pin diameter and stainless-steel (SS) clad thickness are 0.836 cm and 0.057 cm, respectively. The temperature of U-Pu fuel is set to 1123.15 °K, and that of other regions (SS clad, D_2O coolant and shield) is set to 580.15 °K. The calculations have shown that Δk_{eff} $(= k_{eff}^{3D-Pin} - k_{eff}^{RZ})$ is approximately equal to 1500 pcm. Therefore, k_{eff} at the average EOC (33.3 GWd/t) burnup should be around 1.015.

Table 16. Isotopic composition of the MOX fuel.

Isotopes	Pu [wt% of Pu]	Depleted U [wt% of U]
^{238}Pu	0.076	–
^{239}Pu	94.289	–
^{240}Pu	5.306	–
^{241}Pu	0.242	–
^{242}Pu	0.087	–
^{234}U	–	0.0054
^{235}U	–	0.711
^{238}U	–	99.2836

6.1 Equilibrium Fuel Compositions

Figure 15 shows the k_{eff} evolution, calculated by TRITON module of SCALE6.1, until the 17th cycle, in which the core approaches nearly equilibrium condition. The black bold line represents the critical core condition of 3D pin-cell geometry, which is equal to 1.015. The reactivity swing at each cycle decreases as k_{eff} evolves. Figure 16 shows the void coefficients calculated at given burnup state points. As seen in this figure, the void coefficients increase until it reaches the equilibrium cycle. These observations are caused by mainly the increase of necessary total Pu content combined with the decrease in fissile Pu content at the time of the fabrication. The Pu concentration, fissile Pu content (^{239}Pu+^{241}Pu), and the necessary Pu topping at the beginning of cycle are plotted in Figure 17. As seen in this figure, the total Pu mass increases as the evolution of its isotopic compositions, particularly at the earlier stages of cycles (Cycle 1-7). The more detailed mass flows of heavy metals at selected cycles are shown in Tables A-1 – A-5 of Appendix A.

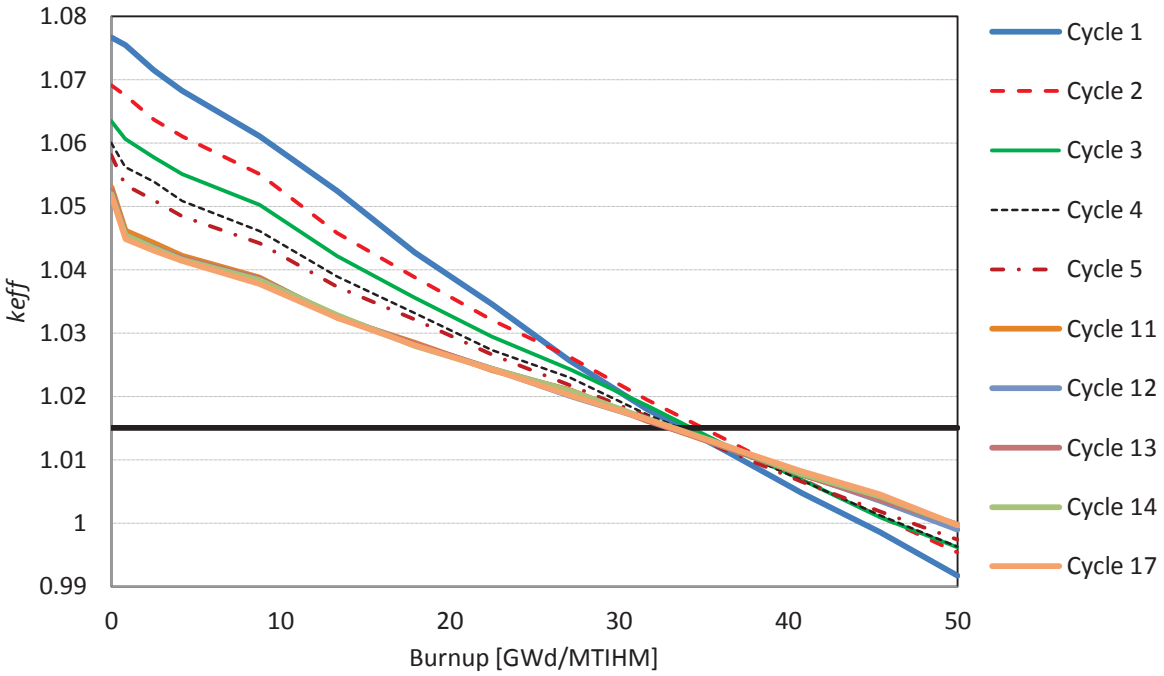

Figure 15. Evolution of k_{eff} until equilibrium. (stdev≅20pcm)

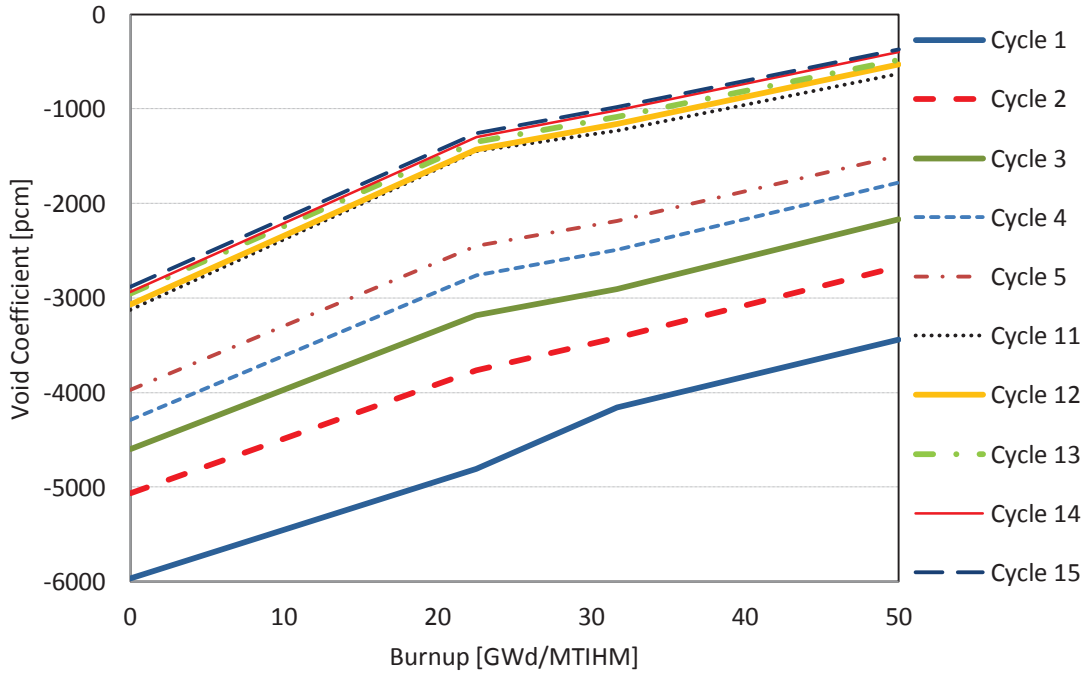

Figure 16. Burnup dependence of void coefficients at each cycle. (stdev≅30pcm)

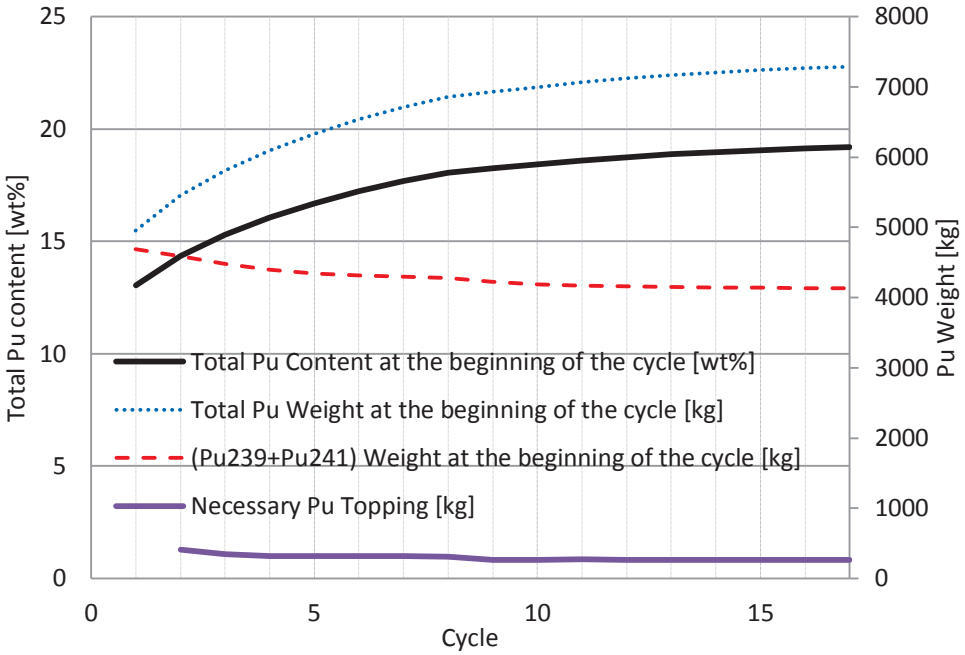

Figure 17. Total Pu content at the beginning of each cycle.

Figures 18a and 18b show the evolution of Pu concentration at fabrication and reprocessing of U-Pu fuel in actual weight (g/pin-cell) and percentage (wt%), respectively. Each spike of curves represents the necessary topping of fresh Pu at the time of the fabrication. Most Pu isotopes reach nearly equilibrium; however, non-fissile ones (i.e., Pu-238 and Pu-240) are still increasing at Cycle 17. Figure 19 shows the relative fissile Pu mass balance, ΔPu_f, at each cycle. ΔPu_f is steadily increasing and reaches around -6% as approaching the equilibrium cycle of 17 because of decrease in the fissile Pu content in the recycled fuel.

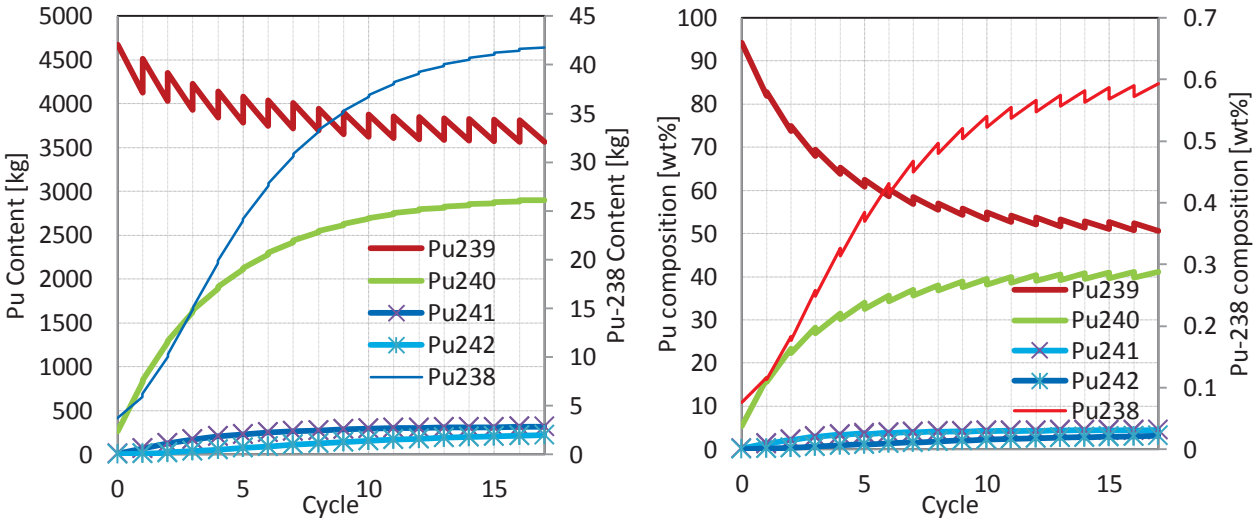

(a) In gram. (b) In weight percentage.

Figure 18. Evolution of Pu concentration at fabrication and reprocessing of the U-Pu fuel.

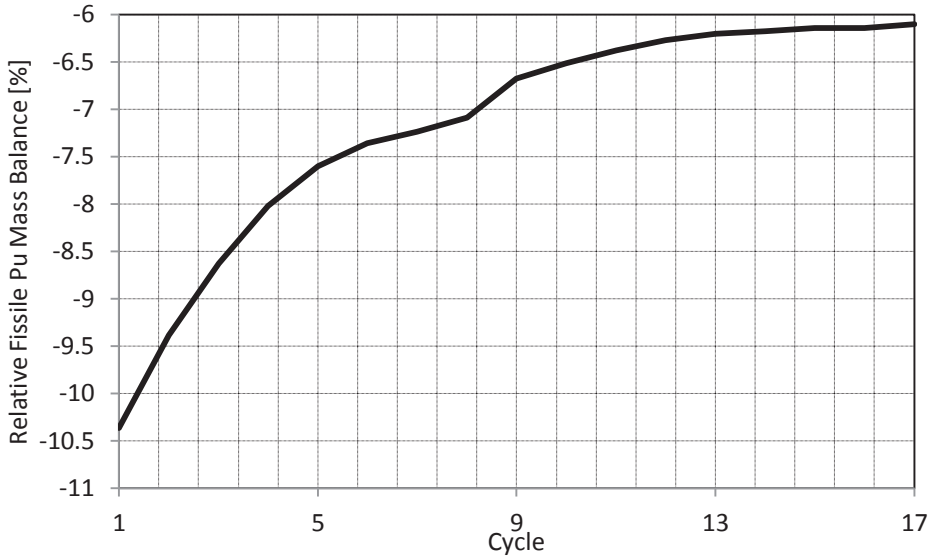

Figure 19. The relative fissile Pu mass balance, ΔPu_f, at each cycle.

So far, we have found that there is also significant impact from the Pu content of the MOX fuel on the core performance. The table below (Table 17) summarizes the core characteristics of selected cycles as well as those obtained by the Pu compositions given by Table 1 (Core 5 in Table 2 of Section 3.2). (Note that for the fair comparison, the Pu enrichment at each cycle are based on the compositions at BOC (after 2 years of aging) since Core 5 of Section 3.2 does not take into account 2 years of aging after the fabrication.) The table indicates that the void coefficient is very sensitive to the initial Pu enrichment such that the higher initial Pu content increases the void coefficient. Pu compositions of Cycles 10 and 15 are close to those in Table 1. The slightly higher fissile Pu mass balances of these two cycles compared to that of the core with Table 1 composition are possibly due to their lower initial ^{241}Pu content.

Table 17. Core characteristics of each cycle.

		Cycle 1	Cycle 5	Cycle 10	Cycle 15	Table 1
Pu enrichment [wt%]		13.05	16.62	18.36	18.98	18.03
Pu compositions [wt%]	^{238}Pu	0.075	0.310	0.498	0.556	2.6
	^{239}Pu	94.315	65.567	55.974	53.136	54.3
	^{240}Pu	5.304	30.301	37.770	39.621	25.9
	^{241}Pu	0.220	2.947	3.731	3.915	8.7
	^{242}Pu	0.087	0.875	2.026	2.771	7.62
ΔPu_f [%]		-10.4	-7.6	-6.5	-6.1	-7.6
Void coefficient [pcm]	BOC	-5965.4	-3972.1	-3195.6	-2885.7	-3636.3
	~18.9 GWd/t	-4807.3	-2450.2	-1561.1	-1255.3	-2403.2
	~32.7 GWd/t	-4156.5	-2183.0	-1290.5	-983.5	-1517.2
	EOC	-3438.1	-1497.7	-657.5	-370.2	-554.2

6.2 Effect of ^{236}U on the Neutronics Performance of D_2O-cooled HCPWRs

In Section 3.2, effect of ^{235}U enrichment in MOX fuel on the Pu conversion ratio has been studied. Such a design choice allows lowering the Pu content in the fuel in order to reach a Pu break-even configuration. As mentioned, the use of enriched uranium increases the production of ^{236}U, in which presence in the recovered uranium decreases the reactivity of fresh MOX fuel because of its capture cross section. In this section, the impact of ^{236}U on the neutronics performance of D_2O-cooled HCPWRs is quantitatively investigated. For this analysis, 60cm core models with FeCrAl cladding (0.4mm thickness with W/F=0.54) discussed in Section 5 are utilized. The MOX fuel is assumed to be fabricated with the plutonium in equilibrium composition given in Table A-5 and enriched uranium with 1 or 2 wt% of ^{236}U. All models take into account 2 years of aging after the fabrication and 5 years of cooling after the irradiation. The enrichments of Pu and U are determined so that the MOX fuel can reach an average burnup at discharge of 51 GWd/t, as well as break-even condition. The Pu fuel-cycle loss of 1.5% is considered, thus the relative fissile mass balance, ΔPu_f, of 1.5% must be attained at the end of each cycle. In order to find ^{235}U enrichment that meets those conditions, plots shown in Figure 20 are created that exhibit relations among initial Pu enrichment, ΔPu_f, and ^{235}U enrichment. According to these plots, it is safe to calculate Pu and ^{235}U enrichments by means of linear interpolations within a range given in these plots.

Table 18 shows Pu and ^{235}U enrichments of each case that can reach 1.5% of ΔPu_f at 51 GWd/t. A slight reduction in Pu enrichment (~0.15 wt%) can be observed as increasing ^{236}U content from 1 to 2 wt%. While this reduction reflects the change in the small amount of fissile Pu (around 50 wt% of total Pu) in the MOX fuel, there is nearly 0.3wt% increase in ^{235}U enrichment as increasing ^{236}U content, which is a significant increase in the fissile content in the MOX fuel. There is also a small penalty in the void coefficient, shown in Figure 21, such that there is approximately 300 pcm increase in void coefficient as increasing ^{236}U content from 1 to 2 wt%.

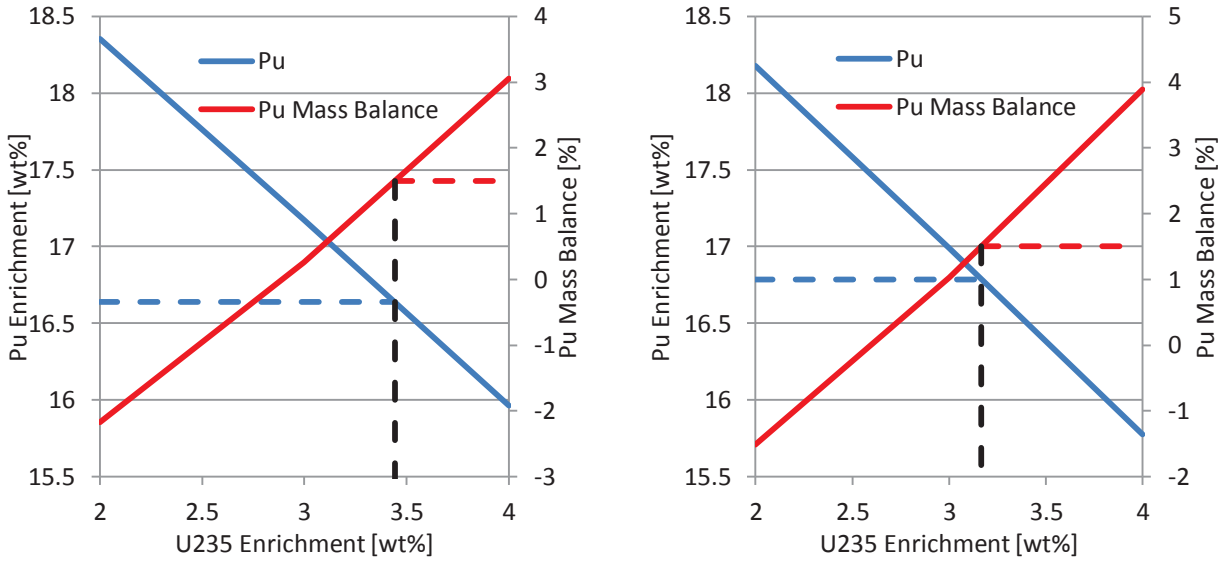

(a) 2 wt% of ^{236}U (b) 1 wt% of ^{236}U

Figure 20. Initial Pu enrichment and ΔPu_f as a function of ^{235}U enrichment for cores (4cm blanket) with 1 and 2 wt% of ^{236}U in the U of the MOX fuel.

Table 18. Pu and ^{235}U enrichments of each case that can reach 1.5% of ΔPu_f at 51 GWd/t.

Axial Blanket Size	Pu Enrichment [wt%]		^{235}U Enrichment [wt%]	
	1 wt% of ^{236}U	2 wt% of ^{236}U	1 wt% of ^{236}U	2 wt% of ^{236}U
0 cm	15.540	15.416	4.211	4.468
2 cm	16.201	16.061	3.682	3.954
4 cm	16.786	16.637	3.167	3.443

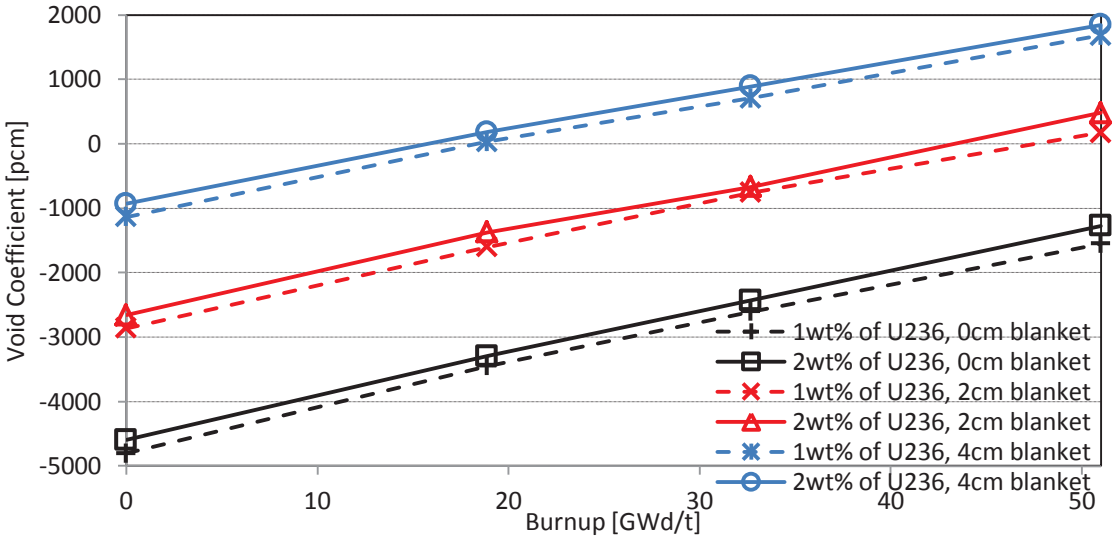

Figure 21. Void coefficients of each core with different ^{236}U content.

7. Analysis of Similarity to Other Reactors Based on Integral Parameter Uncertainties

In this section, we perform sensitivity studies in order to characterize D_2O cooled high-conversion PWRs from different aspects. The goal of the analysis in this section is to quantify the uncertainties of integral parameters (k_{eff} and void coefficients) at different burnup points for other reactor systems to find similarities and trends to D_2O-HCPWR. In the advanced studies, the similarity assessment is performed utilizing a number of experimental systems that well represents the reference system, and these results are applied to the adjustment of system parameters and cross sections for the reduction of uncertainties in the reference system [11-13]. Such data adjustment works are beyond the scope of this paper. We will perform basic assessment of similarities to a few selected systems.

7.1 Modeling and Brief Theoretical Background

We utilize TSUNAMI-3D module in SCALE6.1 [9] for the sensitivity and uncertainty calculations. After the burnup calculation by TRITON module, at selected burnup state points, namely 0, 18.9, 32.7, and 51 GWd/t, 230-250 nuclide compositions from fuel and blanket zones are transferred to the TSUNAMI input decks to perform steady state forward and adjoint calculations for both voided and reference cores. Then, it calculates the sensitivity coefficients for the multiplication factor via the first-order perturbation theory:

$$S_{k_{eff},\Sigma_{\alpha,g}} = \frac{\Sigma_{\alpha,g}}{k_{eff}} \frac{\partial k_{eff}}{\partial \Sigma_{\alpha,g}} \quad , \tag{5}$$

where Σ_α is the macroscopic cross section for reaction α and energy group g. In order to estimate accurate sensitivity coefficients for systems in which resonance self-shielding is important, TSUNAMI has a unique capability for calculating additional terms called implicit sensitivity coefficients given by:

$$S_{\Sigma_{\alpha,g},\omega_i} = \frac{\omega_i}{\Sigma_{\alpha,g}} \frac{\partial \Sigma_{\alpha,g}}{\partial \omega_i} \quad , \tag{6}$$

where ω_i could represent the number density of a particular material, a nuclear data component, or a physical dimension of a system [13,14]. The relative variance of the k_{eff}, ΔR^2, is calculated by:

$$\Delta R^2 = S_k C_{\alpha\alpha} S_k^T , \tag{7}$$

where S_k is the sensitivity vector and $C_{\alpha\alpha}$ is the covariance matrix from 44-group cross section covariance library in SCALE6.1 [9].

Another module called TSAR can calculate sensitivity coefficients for reactivity worth, $\Delta\rho$ using sensitivity coefficients from voided and reference cores:

$$S_{\Delta\rho,\Sigma_\alpha} = \frac{\Sigma_{\alpha,g}}{\Delta\rho} \frac{\partial \Delta\rho}{\partial \Sigma_{\alpha,g}} \quad . \tag{8}$$

TSUNAMI-IP utility module provides us the correlation coefficient that describes the similarity of two different systems based on the uncertainty of integral parameters which is define by:

$$c_k = \frac{\langle S_{k,i}|C_{\alpha,\alpha}|S_{k,j}\rangle^2}{\langle S_{k,i}|C_{\alpha,\alpha}|S_{k,i}\rangle\langle S_{k,j}|C_{\alpha,\alpha}|S_{k,j}\rangle} \quad , \tag{9}$$

where $S_{k,i}$ is the sensitivity coefficient vector of the integral parameter k for the system i. If systems i and j are similar, the value of c_k should be close to 1.0.

7.2 Results and Discussions

For the similarity assessment study respect to D_2O-HCPWR, we have selected PWR (both UOX and MOX fueled), H_2O-HCPWR (the same configuration as D_2O-HCPWR), and sodium cooled fast reactor (SFR). The radial dimension of fuel pins, temperatures, and initial fissile enrichments are given in Table 19. The fuel enrichments of all models have been adjusted to reach 51 GWd/t in 3-batch cores. MOX fuel enrichment is based on the isotopic composition given in Table 1.

Table 19. Summary of 3D-pin burnup models

Parameter	HCPWR	PWR	SFR
Inner D. [cm]	0.836	0.819	0.542
Outer D. [cm]	0.95	0.94	0.655
Core Height [cm]	60	360	60
Fuel Cell	Triangular	Square	Triangular
Pin-Pitch	1.05057	1.25	0.7773
Coolant	H_2O	H_2O	Na
Clad	SS	Zr-4	SS
Fuel Temp [°K]	1123.15	900	1123.15
Clad Temp [°K]	580.15	620	580.15
Coolant Temp [°K]	580.15	575	580.15
Fissile Enrichment [wt%]	11.4 (D_2O) 11.2 (H_2O)	6.3 (MOX) 4.2 (UOX)	13.0

Table 20 shows the relative fissile Pu mass balance, given by Eq. (1), of each system. D_2O-HCPWR has remarkably high Pu conversion capability compared to other reactors. The H_2O-HCPWR has much lower mass balance than D_2O one because of its higher neutron moderation. Table 21 presents correlation coefficients, given by Eq. (9), of k_{eff} for each core respect to D_2O-HCPWR at each burnup state point. As seen in this table, correlation coefficients of k_{eff} are close to one for all reactors except for PWRs. There are two main factors for this difference in correlation factors. One is obviously the neutron spectrum. Since these three types of reactors have harder spectrum than PWR, it shares the common characteristic in uncertainty such that ^{238}U inelastic scattering uncertainty is high. The other factor is the Pu content in the fuel. The reactors except for PWR have high fissile Pu content and less change in the Pu content over the burnup compared to PWR. This is also the reason why UOX fueled PWR has the smallest value but approaches that of MOX fueled PWR as burnup proceeds.

Table 20. Fissile Pu mass balance, ΔPu_f, of each core.

Type of Systems	ΔPu_f [%]
D_2O-HCPWR	-7.62
PWR (MOX)	-29.64
H_2O-HCPWR	-16.09
SFR	-9.47

Table 21. Correlation coefficients of keff for each core respect to D_2O-HCPWR

Burnup [GWd/t]	0	18.9	32.7	51
PWR (UOX)	0.3318	0.6134	0.6486	0.6692
PWR (MOX)	0.7031	0.7133	0.7174	0.7208
H_2O-HCPWR	0.9552	0.9597	0.9614	0.9625
SFR	0.9305	0.9345	0.9377	0.9394

In order to clarify differences observed in above two tables, total (absolute) uncertainties of k_{eff} of each reactor at 0 and 51 GWd/t are plotted in Figures 22a and 22b, respectively, along with their break-up contributions from some of influential reactions. (Note that the square sum of all of break-up contributions will be equal to the square of the total uncertainty). Table 22 shows the calculated k_{eff} at 0 and 51 GWd/t. The major contributors of k_{eff} uncertainties for HCPWRs and SFRs are ^{238}U inelastic and ^{239}Pu nubar whereas only ^{239}Pu nubar and ^{238}U(n,γ) significantly contribute to k_{eff} uncertainty for MOX fueled and UOX fueled PWRs, respectively, since ^{238}U inelastic reaction occurs only at high energy range (larger than 50 keV). Initially ^{238}U(n,γ) uncertainty is the No. 1 contributor of uncertainties in UOX fueled PWR, however, after 51 GWd/t, ^{239}Pu nubar becomes the dominate one since the significant amount of ^{238}U is converted into ^{239}Pu.

Table 22. k_{eff} of each reactor (stdev = ~20pcm)

Burnup [GWd/t]	D_2O-HCPWR	PWR (UOX)	PWR (MOX)	H_2O-HCPWR	SFR
0	1.07416	1.36189	1.13284	1.11431	1.06818
51	0.98718	0.92716	0.96348	0.96954	0.98416

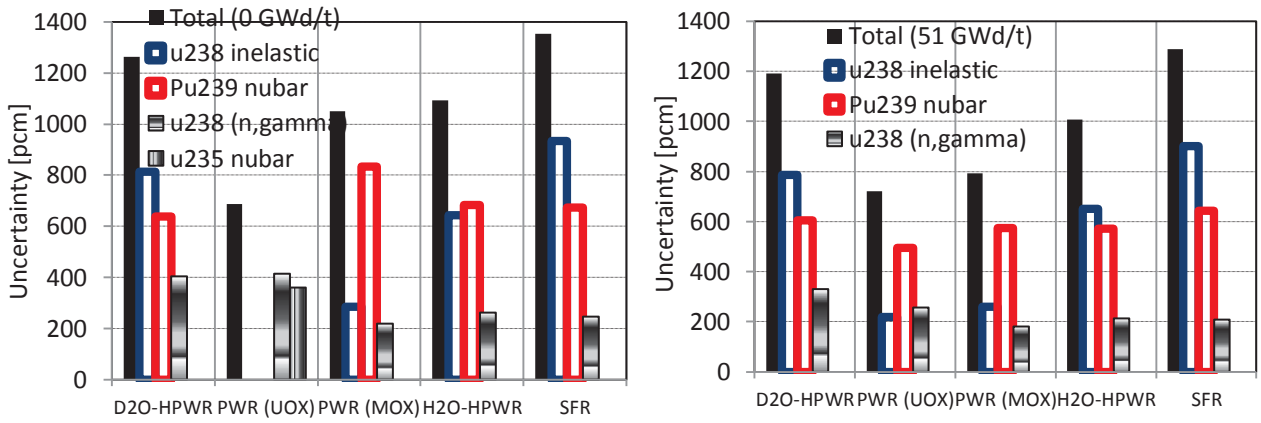

(a) 0 GWd/t (b) 51 GWd/t

Figure 22. k_{eff} uncertainty [pcm] and its reaction-wise contributions

Table 23 shows void coefficients calculated for each reactor at selected burnup points. D_2O-HCPWR has the highest void coefficients of all followed by H_2O cooled HCPWR. Here we can observe that two HCPWRs have the similar trend such that their void coefficients are sensitive to the burnup (void coefficients significantly increase as burnup proceeds.). Such a trend probably reflects into the results of correlation coefficients shown in Table 24. The correlation coefficients of SFR are around 0.7, close to those of PWRs, while those of H_2O-HCPWR still show some similarities having the value around 0.9. Total uncertainties of void coefficients for each reactor at 0 and 51 GWd/t, along with their break-up contributions, are shown in Figures 23a and 23b, respectively. Both PWRs show very high uncertainties in magnitude. However, in percentage these absolute uncertainties correspond to 5-7% for UOX fuel and 14% for MOX fuel. Both D_2O and H_2O HCPWRs have almost invariant uncertainty in their magnitudes through the burnup, 600 pcm and 800 pcm, respectively. Since the void coefficients of HCPWRs increase and approach to zero as burnup proceeds, their percentage uncertainties grow significantly (from 17% to 125% for D_2O and from 11% to 24% for H_2O). The primal contributor of void coefficient uncertainties is ^{238}U inelastic since the large spectrum shift occurs from reference to voided cores, thus it is very sensitive

to the reaction occurs at the high neutron energy range. However, the void coefficient uncertainties for SFR is almost constant in both percentage and absolute values through the burnup (3% and 300 pcm), and Na elastic shows the significant and comparable contribution to other key reactions such as ^{238}U inelastic. Such characteristics somehow differentiate SFR from both HCPWRs and result in smaller correlation values.

Table 23. Void coefficients of each reactor.

Burnup [GWd/t]	D_2O-HCPWR	PWR (UOX)	PWR (MOX)	H_2O-HCPWR	SFR
0	-3640	-68624	-13005	-7287	-9199
18.9	-2380	-79337	-13500	-5642	-9438
32.7	-1469	-90752	-15203	-4578	-9425
51	-495	-106025	-18271	-3452	-9478

Table 24. Correlation coefficients of void coefficient for each core respect to D_2O-HCPWR

Burnup [GWd/t]	0	18.9	32.7	51
PWR (UOX)	0.5805	0.6420	0.6477	0.6580
PWR (MOX)	0.7546	0.7383	0.7196	0.7091
H_2O-HPWR	0.9047	0.9045	0.9002	0.8996
SFR	0.6943	0.7176	0.7027	0.7162

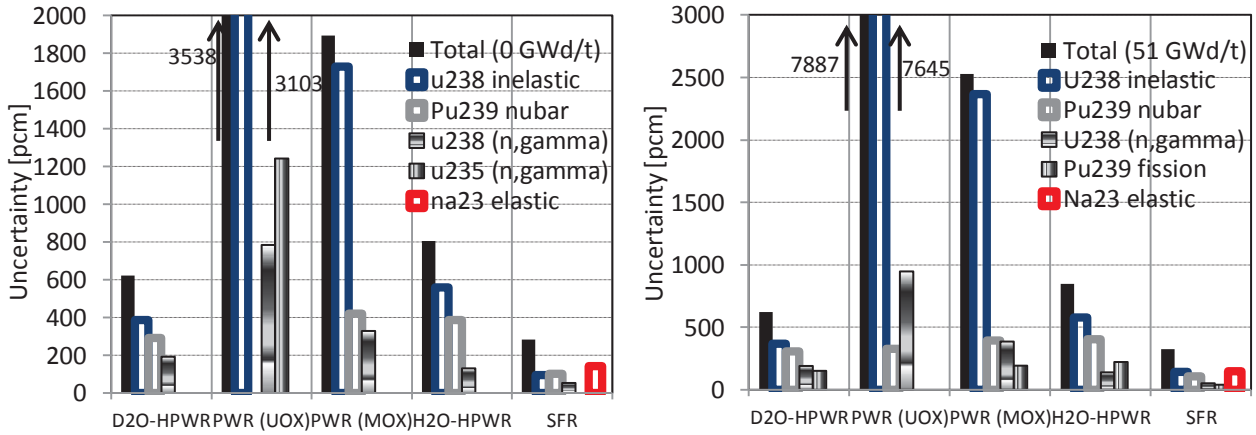

(a) 0 GWd/t (b) 51 GWd/t

Figure 23. Void coefficient uncertainty [pcm] and its reaction-wise contributions.

So far, we have realized the void coefficients of HCPWRs are strongly dependent on the burnup. The plotting of sensitivity coefficient profiles could allow us to identify more detailed contributions. If the sensitivity profiles of key uncertainty contributors shares common parts to those of D_2O-HCPWR, then two systems are considered to be similar. Figure 24 presents normalized sensitivity profiles of ^{238}U inelastic to the void coefficient at 0 GWd/t for SFR, D_2O and H_2O HCPWRs. While sensitivity profiles of both HCPWRs match almost exactly, that of SFR significantly deviates from them. Figure 25 shows sensitivity profiles of ^{239}Pu nubar to the void coefficient at 0 GWd/t. Sensitivity profiles to void coefficient show that they are negatively contributed in the thermal and epithermal ranges whereas those in the higher energy range show the positive contribution. Also the magnitude of contribution is much higher in HCPWRs while it is very small in SFR and PWR.

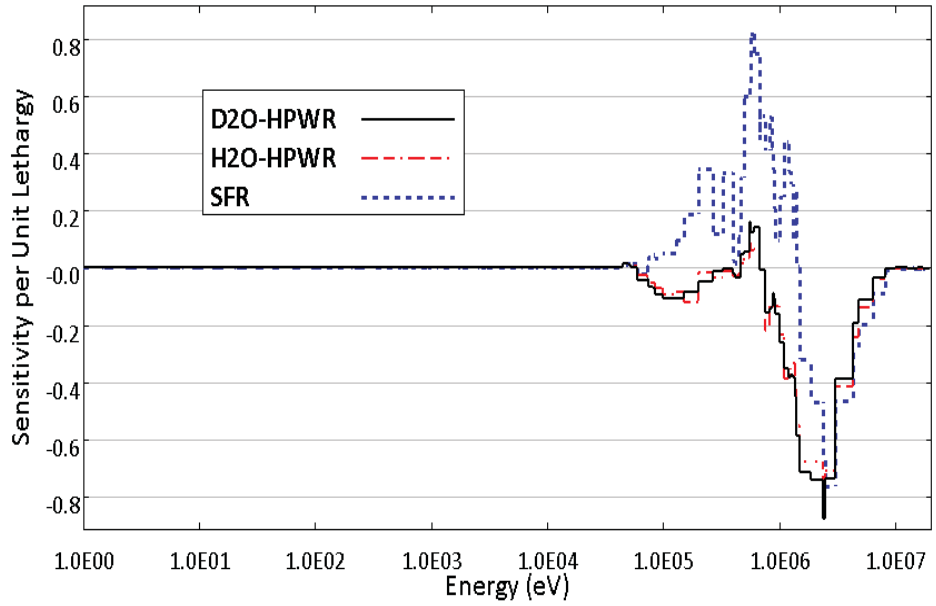

Figure 24. Normalized sensitivity profiles of ^{238}U inelastic to the void coefficient at 0 GWd/t.

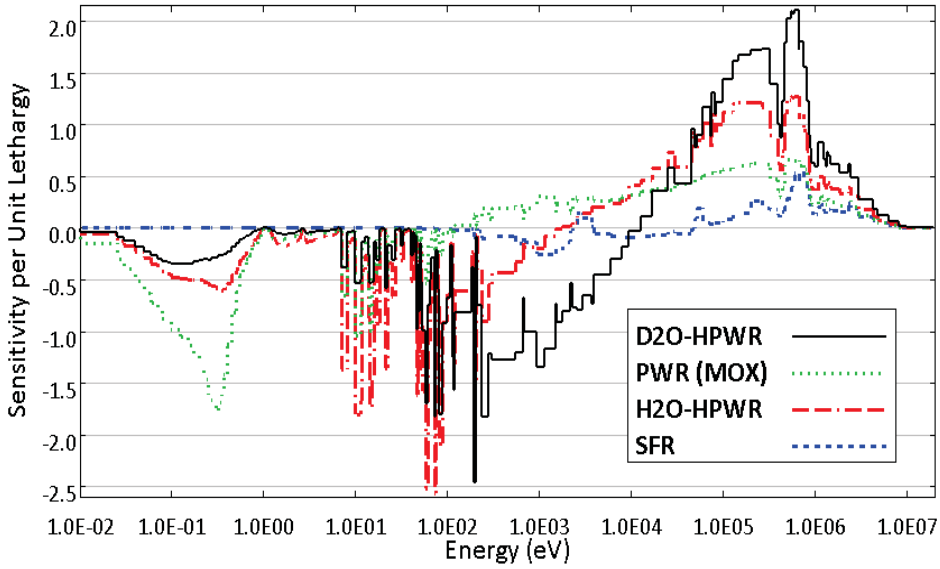

Figure 25. Sensitivity profiles of ^{239}Pu nubar to the void coefficient at 0 GWd/t.

8. Conclusions

This report presented the continuation of the activity started from FY12 and further investigated the D_2O-cooled HCPWRs neutronics design from several aspects. The neutronics analyses of both U-Pu and Th-U fueled cores were carried out in order to obtain fundamental design characteristics of this type of reactors. The analyses focused on the small (or short) sized cores with only axial or internal blanket while aiming at break-even or near-breeder cores and negative void coefficients. SCALE 6.1 code system was utilized, and a series of simple 3D fuel pin-cell models have been developed in order to perform Monte Carlo based criticality and burnup calculations.

The performance of U-Pu fueled cores with axial and internal blankets was analyzed in terms of their impact on the relative fissile Pu mass balance, initial Pu enrichment, and void coefficient. The analyses showed that the relative Pu mass balance was effectively increased by the addition of the axial blanket. The cores having the smallest water-to-fuel ratio (i.e., W/F=0.45) was able to achieve nearly break-even condition by adding 16 cm of axial blanket. However, the void coefficient was strongly sensitive to the presence of the axial blanket. The addition of only 4cm of blanket resulted in the 4000 pcm increase in the void coefficient. Thus, the presence of the axial blanket made the void coefficient hardly negative. On the other hand, the addition of the internal blanket could not effectively increase the Pu mass balance. The initial Pu enrichments were highly sensitive to the presence of the internal blanket. The study showed that the presence of more than 10 cm of internal blanket was capable of reducing the void coefficient. However, the large internal blanket could cause the decoupling of the core and result in an unstable core. None of core configuration was able to attain either break-even or near-breeder condition while retaining the negative void coefficient. In order to achieve the higher Pu conversion, the simulations of the D_2O-coolant boiling were carried out by the set of simple models. The maximum of 1.8% increase in the Pu mass balance was obtained between 40% and 60% of coolant voiding factors. The continued attempts were made in order to improve the Pu conversion through utilizing enriched uranium in the MOX fuel. The analysis showed that MOX fuel with ^{235}U enrichment of around 3.5 wt% can achieve break-even condition without the axial blanket. The addition of axial DU blanket decreases the required ^{235}U enrichment to reach the break-even or breeding conditions, however; significantly increases the void coefficient. The effect of higher and lower target burnups on the conversion performance was also investigated. It was shown that the lower target burnup could help the core to attain both high Pu conversion and negative void coefficient. However, from the fuel cycle view point, the lower target burnup increases the number of reprocessing per unit energy. Thus, it could not be the preferable and economical option considering the reprocessing loss of Pu.

A similar set of analyses were performed for Th-U fueled cores. ^{233}U nuclides were assumed to be initially available in order to estimate the performance of D_2O-cooled high-conversion PWRs. The Th-blanket was accumulated until its total axial length reaches 60cm. As observed in the MOX fueled core, the axial blanket outperformed the internal blanket for ^{233}U mass balance. The addition of the internal blanket was ineffective such that it reduced ^{233}U mass balance while it also decreased the void coefficient with more than 20 cm of internal blanket. The effective conversion performance was obtained in taller cores (80 – 120 cm of axial driver length). The maximum fissile mass balance while retaining the negative void reactivity until the target burnup was around -3.5% which was much higher than the MOX cores (-7.6%) in our investigation. Detailed differences between U-Pu and Th-U fueled cores were analyzed by evaluating the sensitivity coefficients. These sensitivity coefficients indicated that Th-U fueled cores had lower reactivity swing than U-Pu fueled cores, and the fissile mass balance and void coefficients of U-Pu fueled cores were much more sensitive to the change in the initial fissile content in the fuel than those of Th-U fueled cores.

The effect of advanced iron alloy cladding (i.e., FeCrAl) on the performance of Pu conversion in MOX fueled cores was studied instead of using standard stainless-steel cladding. Variations in clad thickness and coolant-to-fuel volume ratio were also exercised. The use of FeCrAl instead of SS as a

cladding alloy reduced the required Pu enrichment and improved the Pu conversion rate primarily due to the absence of nickel in the cladding alloy that resulted in the reduction of the neutron absorption. Also the difference in void coefficients between SS and FeCrAl alloys was nearly 500 pcm over the entire burnup range.

The last part of this report performed sensitivity and uncertainty analyses in order to characterize D_2O cooled HCPWRs from different aspects. The uncertainties of integral parameters (k_{eff} and void coefficient) for selected reactor cores were evaluated at different burnup points in order to find similarities and trends respect to D_2O-HCPWR. TSUNAMI-3D module in SCALE 6.1 was used to perform the sensitivity and uncertainty calculations. The uncertainty analysis of k_{eff} showed that its breakup contributions for D_2O-HCPWR were very similar to other fast systems (SFR and H_2O-HCPWR) such that the key contributors were ^{238}U inelastic and ^{239}Pu nubar. However, breakup uncertainties of void coefficients showed that while those of D_2O-HCPWR resembled to H_2O-HCPWR, Na elastic became the significant contributor of the void coefficient uncertainty of SFR. Also sensitivity profiles of ^{238}U inelastic and ^{239}Pu nubar to the void coefficient revealed that those of SFR were quite dissimilar to both HCPWRs. The study also found that while the absolute values of void coefficient uncertainty for D_2O-HCPWR were invariant through the burnup, its percentage uncertainty was significantly increased. It became 125% at the target burnup of 51 GWd/t. This was caused because the void coefficient of D_2O-HCPWR was very sensitive to the burnup so that it was very small at 51 GWd/t. Such a highly burnup dependent void coefficient could be a unique character of HCPWRs and an important point to consider for its realistic design. While the uncertainty calculations in this paper were performed for the simple similarity assessment to other types of reactors, detailed comparisons to existing systems will be useful for the construction of the nuclear group data that reduce the uncertainties of D_2O-HCPWRs.

9. References

1. K. Hibi, S. Shimada, T. Okubo, T. Iwamura, and S. Wada, "Conceptual designing of reduced-moderation water reactor with heavy water coolant," *Nucl. Eng. Design*, **210**, 9-19 (2001).
2. A. Radkowsky, "A Heavy Water Breeder Conceptual Core Design," EPRI NP-2176, RP712-1, Final Report, December 1981.
3. T. Downer, et al., "Technical Evaluation of the Hitachi Resource-Renewable BWR (RBWR) Design Concept," EPRI, Palo Alto, CA: 2012, 1025086.
4. G. Youinou and I. Somoza, "Improving Natural Uranium Utilization by Using Thorium in Low Moderation PWRs – A Preliminary Neutronic Scoping Study," *INL/EXT-10-20155*, October 2010.
5. S. Permana, N. Takaki, and H. Sekimoto, "Breeding Capability and Void Reactivity Analysis of Heavy-Water-Cooled Thorium Reactor," *J. Nucl. Sci. Technol.*, Vol. 45, No. 7, p. 589-600 (2008).
6. V. Vallet, B. Gastaldi, J. Politello, A. Santamarina, and L. Van Den Durpel, "Introduction of Thorium-Based Fuels in High Conversion Pressurized Water Reactors," *Nucl. Technol*, **182**, 187-206 (2013).
7. Y. Shaposhnik, E. Shwageraus, and E. Elias, "Core Design options for High Conversion BWRs operating in Th-^{233}U Fuel Cycle," *Nucl. Eng. Design*, **263**, 193-205, (2013).
8. H. Hiruta and G. Youinou, "Preliminary Neutronics Design and Analysis of D2O Cooled High Conversion PWRs," INL/EXT-12-27316, September 2012.
9. *Scale: A Comprehensive Modeling and Simulation Suite for Nuclear Safety Analysis and Design*, ORNL/TM-2005/39, Version 6.1, June 2011. Available from Radiation Safety Information Computational Center at Oak Ridge National Laboratory as CCC-785.
10. K. A. Terrani, S. J. Zinkle, and L. L. Snead, "Advanced Oxidation-Resistant Iron-Based Alloys for LWR Fuel Cladding," *J. Nucl. Mater*. (2013), http://dx.doi.org/10.1016/j.jnucmat.2013.06.041 (in press).
11. G. Palmiotti and M. Salvatores, "Use of Integral Experiments in the Assessment of Large Liquid-Metal Fast Breeder Reactor Basic Design Parameters," *Nucl. Sci. Eng.*, **87**, 333 (1984).
12. G. Palmiotti, et al., "A Global Approach to the Physics Validation of Simulation Codes for Future Nuclear Systems," *PHYSOR 2008, Int. Conf. on Reactor Physiscs, Nuclear Power: A Sustainable Resource, Interlaken*, Switzerland, September 14-19, 2008.
13. B. L. Broadhead, B. T. Rearden, C. M. Hopper, J. J. Wagschal, and C. V. Parks, "Sensitivity- and Uncertainty-Based Criticality Safety Validation Techniques," *Nucl. Sci. Eng.*, **146**, 340-366 (2004).
14. M. L. Williams, B. L. Broadhead, and C. V. Parks, "Eigenvalue Sensitivity Theory for Resonance-Shielded Cross Sections," *Nucl. Sci. Eng.*, **138**, 177 (2001).

Appendix A

Isotopic Compositions HCPWR MOX Fuel until Equilibrium Cycle

Table A-1. Isotopic composition (wt%) of HCPWR MOX fuel at Cycle 1.

Isotope	BOC - 2 years of aging	BOC	EOC	EOC + 4 years of cooling
^{234}U	0.00470	0.00485	0.00422	0.00483
^{235}U	0.61817	0.61918	0.35433	0.35581
^{236}U	0.00000	0.00014	0.06698	0.06810
^{238}U	86.32328	86.32524	81.07494	81.06452
^{238}Pu	0.00992	0.00976	0.01507	0.01553
^{239}Pu	12.30832	12.30860	10.86743	10.87603
^{240}Pu	0.69269	0.69220	2.18038	2.17910
^{241}Pu	0.03158	0.02867	0.23424	0.18381
^{242}Pu	0.01135	0.01135	0.02396	0.02396
^{237}Np	0.00000	0.00000	0.02776	0.02840
^{241}Am	0.00000	0.00000	0.02008	0.07012
^{242m}Am	0.00000	0.00000	0.00048	0.00047
^{243}Am	0.00000	0.00000	0.00393	0.00393
^{243}Cm	0.00000	0.00000	0.00004	0.00004
^{244}Cm	0.00000	0.00000	0.00095	0.00079
^{245}Cm	0.00000	0.00000	0.00007	0.00007
FP	0.00000	0.00000	5.12514	5.12451

Table A-2. Isotopic composition (wt%) of HCPWR MOX fuel at Cycle 5.

Isotope	BOC - 2 years of aging	BOC	EOC	EOC + 4 years of cooling
^{234}U	0.00450	0.00531	0.00567	0.00813
^{235}U	0.59265	0.59320	0.34498	0.34632
^{236}U	0.00000	0.00105	0.06487	0.06774
^{238}U	82.72130	82.72825	77.72825	77.71368
^{238}Pu	0.05236	0.05157	0.05908	0.06305
^{239}Pu	10.90281	10.89872	9.95664	9.96577
^{240}Pu	5.04130	5.03672	5.56303	5.55998
^{241}Pu	0.53964	0.48987	0.77078	0.60460
^{242}Pu	0.14544	0.14545	0.19359	0.19357
^{237}Np	0.00000	0.00008	0.02732	0.02920
^{241}Am	0.00000	0.04979	0.11995	0.28414
^{242m}Am	0.00000	0.00000	0.00384	0.00374
^{243}Am	0.00000	0.00000	0.02707	0.02706
^{243}Cm	0.00000	0.00000	0.00034	0.00030
^{244}Cm	0.00000	0.00000	0.00592	0.00489
^{245}Cm	0.00000	0.00000	0.00039	0.00039
FP	0.00000	0.00000	5.12829	5.12741

Table A-3. Isotopic composition (wt%) of HCPWR MOX fuel at Cycle 10.

Isotope	BOC - 2 years of aging	BOC	EOC	EOC + 4 years of cooling
^{234}U	0.00441	0.00584	0.00701	0.01079
^{235}U	0.58027	0.58076	0.33961	0.34089
^{236}U	0.00000	0.00144	0.06400	0.06766
^{238}U	80.98802	80.98633	76.11604	76.10122
^{238}Pu	0.09289	0.09144	0.09199	0.09663
^{239}Pu	10.27482	10.27461	9.52905	9.53620
^{240}Pu	6.93325	6.93311	7.07350	7.07112
^{241}Pu	0.75435	0.68481	0.98470	0.77241
^{242}Pu	0.37197	0.37197	0.40863	0.40855
^{237}Np	0.00000	0.00011	0.02711	0.02950
^{241}Am	0.00000	0.06958	0.16172	0.37139
^{242m}Am	0.00000	0.00000	0.00519	0.00507
^{243}Am	0.00000	0.00000	0.05102	0.05100
^{243}Cm	0.00000	0.00000	0.00046	0.00041
^{244}Cm	0.00000	0.00000	0.01072	0.00885
^{245}Cm	0.00000	0.00000	0.00069	0.00069
FP	0.00000	0.00000	5.12856	5.12761

Table A-4. Isotopic composition (wt%) of HCPWR MOX fuel at Cycle 15.

Isotope	BOC - 2 years of aging	BOC	EOC	EOC + 4 years of cooling
^{234}U	0.00437	0.00603	0.00749	0.01172
^{235}U	0.57555	0.57606	0.33772	0.33900
^{236}U	0.00000	0.00156	0.06362	0.06752
^{238}U	80.35669	80.35899	75.51881	75.50542
^{238}Pu	0.10731	0.10561	0.10333	0.10811
^{239}Pu	10.08584	10.08613	9.40237	9.40970
^{240}Pu	7.52563	7.52084	7.54889	7.54455
^{241}Pu	0.81857	0.74308	1.04866	0.82266
^{242}Pu	0.52604	0.52606	0.54714	0.54704
^{237}Np	0.00000	0.00012	0.02699	0.02954
^{241}Am	0.00000	0.07551	0.17442	0.39770
^{242m}Am	0.00000	0.00000	0.00559	0.00546
^{243}Am	0.00000	0.00000	0.06525	0.06522
^{243}Cm	0.00000	0.00000	0.00049	0.00043
^{244}Cm	0.00000	0.00000	0.01351	0.01116
^{245}Cm	0.00000	0.00000	0.00086	0.00086
FP	0.00000	0.00000	5.13487	5.13390

Table A-5. Isotopic composition (wt%) of HCPWR MOX fuel at Cycle 17 (Equilibrium Cycle).

Isotope	BOC - 2 years of aging	BOC	EOC	EOC + 4 years of cooling
^{234}U	0.00437	0.00606	0.00756	0.01187
^{235}U	0.57473	0.57522	0.33727	0.33851
^{236}U	0.00000	0.00158	0.06356	0.06750
^{238}U	80.23245	80.23076	75.41418	75.39908
^{238}Pu	0.10974	0.10799	0.10520	0.11002
^{239}Pu	10.04906	10.04885	9.37282	9.38094
^{240}Pu	7.63309	7.63293	7.63445	7.63092
^{241}Pu	0.82934	0.75279	1.05949	0.83128
^{242}Pu	0.56723	0.56722	0.58351	0.58339
^{237}Np	0.00000	0.00012	0.02695	0.02953
^{241}Am	0.00000	0.07648	0.17651	0.40212
^{242m}Am	0.00000	0.00000	0.00566	0.00552
^{243}Am	0.00000	0.00000	0.06879	0.06878
^{243}Cm	0.00000	0.00000	0.00050	0.00044
^{244}Cm	0.00000	0.00000	0.01423	0.01175
^{245}Cm	0.00000	0.00000	0.00091	0.00091
FP	0.00000	0.00000	5.12841	5.12743